JOURNAL OF GEOPHYSICAL RESEARCH, VOL. 90, NO. A3, PAGES 2673-2694, MARCH 1, 1985

AN EXPLANATION FOR THE H LY α LONGITUDINAL ASYMMETRY IN THE EQUATORIAL SPECTRUM OF JUPITER: AN OUTCROP OF PARADOXICAL ENERGY DEPOSITION IN THE EXOSPHERE

D. E. Shemansky[1]

Center for Space Sciences, University of Southern California, Tucson, Arizona

Abstract. An analysis of the Voyager EUV spectra of the Jupiter sunlit equatorial emissions shows no evidence for a substantial dependence of atomic hydrogen abundance on magnetic longitude, required by earlier theories of the H Ly α longitudinal asymmetry. An explanation for the H Ly α bulge phenomenon is advanced in this work that conforms to the observations and does not require a strong asymmetry in atomic hydrogen abundance. It is proposed that the H Ly α bulge is caused by a combination of proton collisional transfer of H(2s) atoms into the H(2p) state, and production through recombination of H_2^+ and H_3^+, in an asymmetric ionosphere. The asymmetry in the ionosphere is presumably caused by Jupiter's magnetic anomaly. The processes producing the H Ly α bulge require a negligible amount of directly applied energy. However, the phenomenon is a symptom of a process of substantial deposition of energy in the exosphere, forming the major source for ionospheric particles and contributing substantially to the upper atmospheric temperature. According to the present model a large fraction of the observed H Ly α emission from the equatorial region is electron excited, at least at times of solar maximum. Other related phenomena and quantities required to maintain the H Ly α asymmetry are discussed in the text.

Introduction

Sandel et al. (SBS) [1980] describe the observation of a phenomenon in H Ly α emission from Jupiter's atmosphere that seems to be unique to that planet. The low latitude emission of Ly α radiation shows a distinct bulge associated with magnetic longitude, having a broad peak near 110° λ_{III} [1965] with full width half maximum (FWHM) of ~125°. The brightness of the bulge had a measured amplitude ~5 kR above a background of ~14 kR in the equatorial region of the sunlit atmosphere. The asymmetry apparently is persistent, since according to SBS, it was present with similar magnitude and longitudinal position over the 4-month interval between Voyager spacecraft encounters, and has been observed in International Ultraviolet Explorer (IUE) data over a period of three years [Clarke et al., 1980a; Skinner et al., 1983].

A very simple explanation of the bulge, preferential energetic particle precipitation over a particular range of longitude, has been discounted by SBS as a direct excitation process because a similar increase in the H_2 EUV band emission measured simultaneously with Ly α was not detected. The EUV equatorial emission characteristics from Jupiter at the time of Voyager encounters thus have the following general description. The sunlit atmosphere near the equator at the central meridian produced an H Ly α intensity near 14 kR with a bulge rising to ~20 kR at 110° λ_{III}. At the same time, emission in H_2 Lyman and Werner bands was nearly constant at ~3 kR. On the other hand the equatorial darkside atmosphere produced ~800 R of H Ly α emission, but no other detectable radiative source.

Given the facts described above, SBS concluded that the H column density above the 110° longitude region must be enhanced over the abundance in the 200° - 300° region, and resonance scattering of the solar line simply followed the bulge in abundance. In a more detailed discussion along the lines suggested by SBS, Dessler et al. [1981] (DSA) describe a bulge in atomic hydrogen postulated to be produced by asymmetric inward convection of high-energy particles in a theoretical two-cell magnetospheric pattern [see Vasyliunas and Dessler, 1981]. An alternative explanation by Clarke et al. [1981] suggests a centrifugally driven flow of atomic hydrogen generated in the auroral zones, but this would not easily explain the H Ly α brightness contour conformation to the particle drift equator (DSA) shown by the Voyager data.

All of the published discussions of the H Ly α bulge have therefore centered on the assumption that the variation in emission is caused by a resonance-scattered solar line in an atmosphere showing longitudinal variation in H abundance. It has been generally recognized both by the authors of the early papers (SBS, DSA) and by others [Waite et al., 1983] that the proposed solution is seriously flawed. These questions are discussed further in this paper, and it is proposed that the postulation of an atomic hydrogen longitudinal abundance asymmetry is not plausible on several grounds. Of particular importance is the fact that a detailed analysis of the Voyager observations as presented below shows direct evidence that the atomic hydrogen abundance is essentially constant in longitude, although the new analysis agrees with the other basic observational results as presented by SBS. A number of hydrogen reactions are examined in the present paper with the purpose of explaining the bulge phenomenon, and it is suggested that the only plausible explanation of the process conforming with the observational facts lies in the transfer of H atoms in the 2s state into the 2p state in a preferred magnetic longitude region, coupled with variable recombination of H_3^+ and H_2^+. It is proposed that the H Ly α bulge is indeed associated with the magnetic anomaly on Jupiter but the mechanism is vastly different from the concept of a mountain of atomic hydrogen as described by Hill et al.

[1]Now at Lunar and Planetary Laboratory, University of Arizona, Tucson.

Paper number 4A8207.
0148-0227/85/004A-8207$05.00

[1983], and does not involve the transfer of large amounts of energy as implied by the earlier work.

One of the more important results of the data analysis presented here is the placement of the H_2 band emission mean source altitude in the exobase. The H_2 spectra are very similar to the Saturn dayside equatorial emissions [Shemansky and Ajello, 1983 (SA)]. The kinetic energy deposition rate implied by the Saturn emission accounts for the upper atmospheric temperature (400 K) [Shemansky and Smith, 1982; Smith et al., 1983; Shemansky and Smith, manuscript in preparation, 1984]. It appears likely that the analogous process on Jupiter may account for the 1000-K upper atmospheric temperature. The high altitude of the H_2 electron excitation on Jupiter is the basic condition allowing the production of the H Ly α bulge, according to the present analysis. The same phenomenon is not observed on Saturn because of the higher degree of symmetry in the Saturnian magnetic field. The underlying mechanism generating the high-altitude emission on both planets is not understood and poses a problem of fundamental importance because the implied energy deposition must be produced internally in each case. The following text is confined primarily to the explanation of the Jupiter H Ly α bulge. The more important question, of how substantial amounts of particle energy are deposited in the exosphere by an internal transformation of energy, is discussed briefly below, but more detailed study is left to the future.

Observational Results

The observational data applied to the analysis in the present work are the same as those described by SBS and DSA. However, in this case the detailed reduction process is restricted to the Voyager 2 (V2) north-south and east-west maps (see SBS). Details of longitudinal and latitudinal structure of the H Ly α brightness are not examined here, because the results in the new analysis are in basic agreement with the earlier work. The concern in this paper is with the exact nature of the processes inferred from the comparison of the bulge/antibulge spectra. Figures 1 and 2 show superposed plots of averaged bulge and antibulge spectra obtained from the N-S and E-W maps respectively. The solar phase angle is about 17° for this preencounter period. The spectra, given in instrument absolute count rates, show the basic facts related to the bulge phenomena. Figures 1a and 2a show the enhancement of the H Ly α line in the λ_{III} 110° region in the N-S and E-W maps. The N-S map spectra (Figure 1a) show a greater difference in H Ly α intensity basically because the E-W map data represent an average over a broader range of longitudes. Figures 1b and 2b contain the same spectra scaled up to show the superposition of the H_2 emission spectra. These spectra have been reduced through the subtraction of noise background and foreground signals from the Io plasma torus. The contamination of the spectra with foreground Io plasma torus emission is removed through subtraction of a spectrum from direct observations of the torus plasma. The foreground contamination is relatively weak, and the stronger torus signals occur in the 600 to 850-Å region, where Jupiter equatorial emission is weak and not relevant to the modeling process. The noise background signal is composed of a combination of a constant component (~0.02 counts s^{-1} $Channel^{-1}$) now recognized as originating from the radioisotope thermoelectric generators (RTG) on the spacecraft [cf. Broadfoot et al., 1981], and a variable component produced by energetic particles in Jupiter's magnetosphere. The spectra shown here were obtained inside a range of 80 R_J from the planet, and the latter component tends to dominate the noise background. The magnetospheric component of the noise signal has a dependence on magnetic longitude both in spectral shape and magnitude, mostly because of the longitudinally varying position of the spacecraft relative to the magnetic equator. It is therefore necessary to carefully apply noise background spectra from specific longitude regions in the reduction process. Internal instrumental photon scattering has also been removed from the spectra shown here through the application of a recently refined scattering matrix to the spectral data vector [see Broadfoot et al., 1981].

There are a number of visually distinct characteristics in the spectra of Figures 1 and 2, apart from the obvious differences in H Ly α intensity. The emissions in the 500 to 1675-Å band pass of the bulge/antibulge spectra are equal within statistical uncertainty with the exception of the features at ~920 to 950-Å and 1025-Å. Both the N-S and E-W spectra in Figures 1b and 2b have consistently stronger signals at these wavelengths in the antibulge data, showing a tendency opposed to the longitudinal variation of the H Ly α signal. The helium resonance line at 584-Å in both data sets appears to be constant in bulge/antibulge longitudes within statistical uncertainty. This result is in direct disagreement with the analysis of the same data shown by McConnell et al. [1981] (MSB). The latter suggested an He 584-Å longitudinal dependence in opposition to the H Ly α variation. However, the earlier MSB work did not apply the reduction technique discussed above, and noise background spectra were not actually subtracted from the spectra. It is suggested that the longitudinal variation of background noise may have contaminated the MSB He 584-Å emission rate estimates, and this feature is in fact constant in magnetic longitude. The H_2 Rydberg band systems dominate the spectrum from just shortward of 800-Å to 1500-Å. The bands are obviously excited by electron impact, as discussed below, and can be accurately modeled [Shemansky and Ajello, 1983; Ajello et al., 1984]. It should be noted that the N-S map data (Figure 1b) give the appearance of having a significantly greater noise structure than the E-W map data of Figure 2b. This difference is the direct result of a greater noise background in the N-S data because of closer proximity to the planet, rather than any differences in integration time. The spectral region longward of 1250-Å is especially sensitive to the energetic magnetospheric particles and hence we have the distinctly noisy structure in the 1250 to 1500-Å region of Figure 1b. The model calculations discussed below include electron-excited atomic hydrogen, which produces measurable Rydberg series emissions in the 911 to 1025-Å region and at 1216-Å. The intensity differences in the

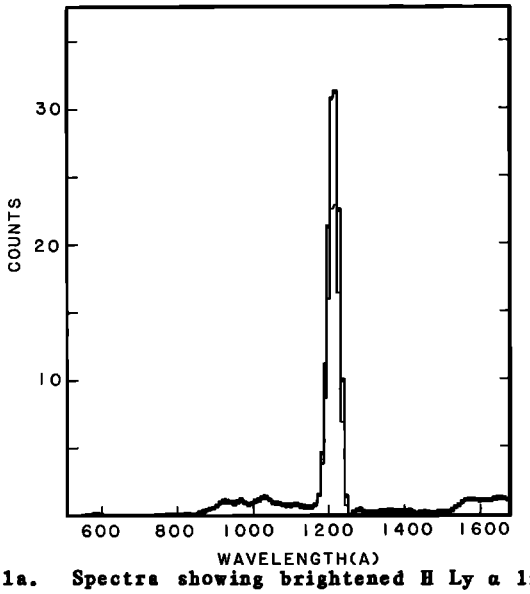

Fig. 1a. Spectra showing brightened H Ly α line in the bulge spectrum.

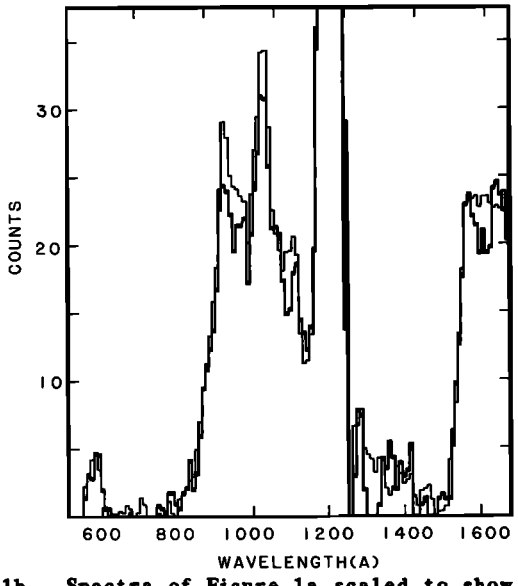

Fig. 1b. Spectra of Figure 1a scaled to show the H_2 Rydberg systems, He (584 Å) line, and solar continuum reflection spectrum (>1500 Å). See text.

Fig. 1. Voyager 2 EUV spectra of the Jupiter subsolar equatorial region, obtained from the preencounter north-south (N-S) map sequence day 188, 1979. The heavy line is the spectrum obtained in the H Ly α bulge region, ~±30° latitude, ~110° λ_{III} longitude, in the subsolar region. The light line is the spectrum in the antibulge subsolar region. The spectra are scaled to the same temporal integration interval. Spacecraft-planet-sun angle ~17°.

bulge/antibulge data at ~920-Å and 1025-Å as noted above are attributed to the e + H reaction in the modeling process, whereas the blended H_2 band intensities are constant within measurement accuracy. The strong emission longward of 1500-Å is attributed, with a weak contribution from H_2 bands, to the reflection spectrum of the solar continuum which rises strongly toward longer wavelengths in this region [Gladstone and Yung, 1983]. The solar continuum reflection spectrum is constant in respect to magnetic longitude within measurement uncertainty.

Figures 3 and 4 show superpositions of the N-S and E-W data in the bulge (Figure 3) and antibulge (Figure 4) regions. These figures illustrate the essential facts relative to the center to limb variation of the emission features, because the N-S map data represent emission rates near the subsolar point, whereas the E-W map data represent uniform averages over the limb-to-center-to-limb equatorial region. Therefore emission features controlled by the scattering of solar radiation will tend to be weaker in the E-W map measurements compared to the N-S subsolar data. The

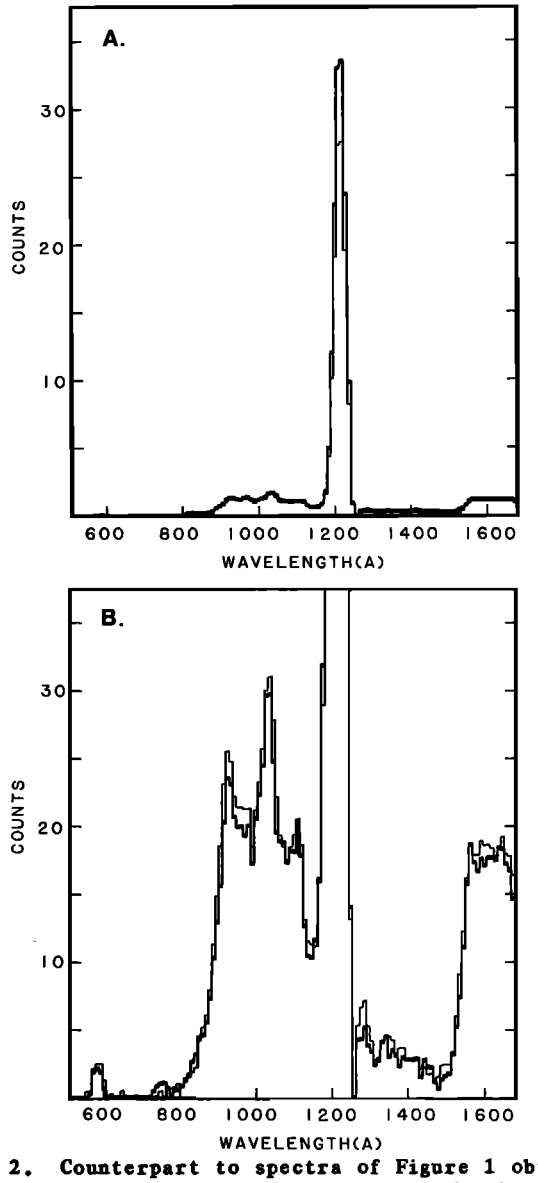

Fig. 2. Counterpart to spectra of Figure 1 obtained from the Voyager 2 east-west (E-W) map sequence day 187, 1979. The spectra are averages over the dawn to dusk equatorial region at H Ly α bulge and antibulge λ_{III} longitudes. The bulge brightening effect is somewhat diluted by averaging over a broader range of magnetic longitude.

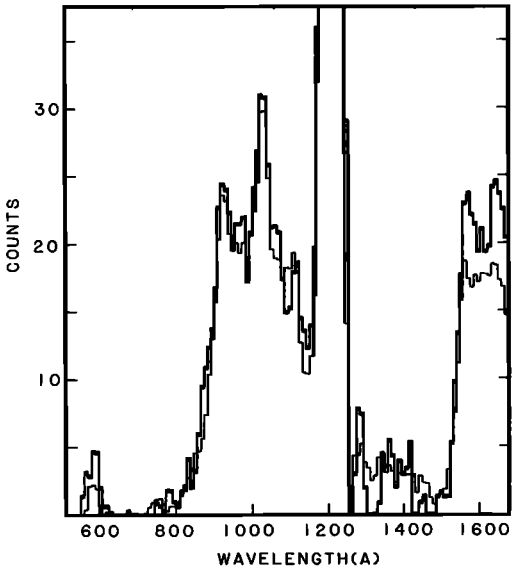

Fig. 3. Superposed spectra of the N-S and E-W maps of Figures 1 and 2, obtained at the magnetic longitudes of the H Ly α bulge. The brightness of the H_2 Rydberg bands in the 800- to 1600-Å region from the N-S map shown as a heavy line is almost identical to that of the E-W map. Strong differences in the intensity of the He 584-Å line and the solar reflection spectrum (1500 - 1674 Å) appear because of limb darkening effects included in the E-W map dawn to dusk averaging of the sunlit equatorial emission. The H_2 Rydberg bands apparently are not affected by limb darkening, and the only N-S versus E-W difference that appears is a weak effect attributed to H_2 foreground abundance (see Figures 8 and 9).

most striking differences are in the intensity of the He 584-Å line, and the solar reflection continuum, visually obvious in Figures 3 and 4. On the other hand the H_2 band emission brightness is almost exactly the same in the N-S versus E-W spectra, suggesting that the subsolar point shows the same brightness as the limb-to-center-to-limb average. The H Ly α intensity shows only moderate change between N-S and E-W map averaged data. Details of the dusk-dawn intensity dependences will be discussed in the next section, because of the obvious importance of these characteristics to an understanding of the energy deposition phenomenon.

Characteristics of the Excited Atmospheric Particles

The emission spectra shown in Figures 1-4 require some combination of solar radiation and electrons as energy sources for the excitation of the atmospheric particles. The interaction of solar radiation with Jupiter's atmosphere produces resonance-scattered radiation from the He and H resonance lines and fluorescence in the H_2 Rydberg bands. Resonance scattering in the He 584-Å line appears to be the dominant source in the observed spectrum from the equatorial region (see MSB). The H Ly α line has been generally assumed to be produced entirely by solar resonance scattering. This assumption is based on the consideration that the production of photoelectrons by solar radiation in the required energy range occurs too deep in the atmosphere to provide a significant e + H source. However, the present analysis shows a quite different result, and it will be shown that a substantial fraction of the 1216-Å line is produced by electron excitation, and the emission does not follow a cosine center to limb variation. Fluorescence of the H_2 Rydberg bands is caused by the accidental near coincidence of the H Ly β 1025.72-Å line with the H_2 Lyman (6,0) P(1) 1025.94-Å line. However, the intensity produced in band fluorescence is orders of magnitude weaker than the observed emission and is not included in the present modeling process.

Accurate models of electron-excited H_2 Rydberg bands have been developed and applied to planetary and laboratory data [Shemansky and Ajello, 1983; Ajello et al., 1984]. Seven band systems, B-X, B'-X, B''-X, E,F-B, C-X, D-X, and D'-X account for virtually all of the observed EUV emission from singlet electronic states [Ajello et al., 1984]. The e + H_2 model described by Shemansky and Ajello [1983] has been improved by the inclusion of predissociation effects and the application of electron temperature dependence in the excitation process. The shape of the observed spectrum depends on two physical parameters in the calculations, the abundance of the H_2 foreground gas and the energy distribution of the exciting electrons. The equatorial spectra of Jupiter and Saturn never show effects of hydrocarbon absorption, in contrast to some auroral spectra. The effect of self-absorption in the foreground H_2 in the model calculation is shown in the predicted instrument response given in Figure 5. The self-absorption process predominantly affects the region shortward of 1000-Å

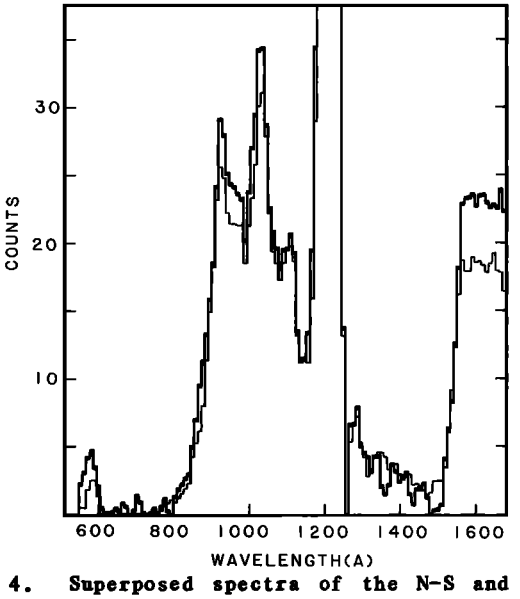

Fig. 4. Superposed spectra of the N-S and E-W maps of Figures 1 and 2, obtained at antibulge magnetic longitudes. Differences between the spectra are similar to those of Figure 3, but emission at 920 Å and 1025 Å is slightly enhanced in the N-S map spectrum, suggesting small differences in the atomic hydrogen contribution to the spectrum.

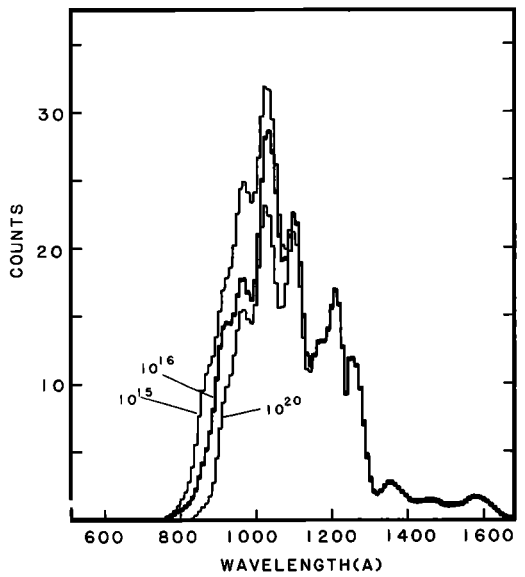

Fig. 5. Model calculations of the H_2 Rydberg system, giving predicted signal for the Voyager 2 ultraviolet spectrometer (UVS) instrument. The calculations show the effect of the abundance of H_2 gas between source and observer. The three curves shown are calculated for abundances of $[H_2]\ell$ = 10^{15}, 10^{16}, and 10^{20} cm^{-2}. The shape and spectral location of the short-wavelength emission are used to estimate the foreground abundance in the observed data. Abundances greater than $[H_2]\ell$ = 10^{20} cm^{-2} are difficult to detect due to saturation of most of the H_2X (v = 0) connected lines.

(Figure 5), and the shape of the bands in this region can be used to estimate the mean altitude of the atmospheric source. Abundances greater than $[H_2]\ell$ = 10^{20} cm^{-2} are difficult to measure by this method because of the tendency toward total saturation of most of the absorbing transitions. It is assumed in these calculations that the ground state vibrational levels are near thermal equilibrium. Figure 6 shows the effect of electron temperature, which is mainly detectable in the modeled spectrum in variability of the feature near 1330-Å, caused by variation in the E,F-B cascade component in the Lyman band system. Changes in the spectrum are generally not detectable at electron temperatures above T_e = 3 x 10^6 K. The observation of various sources has shown variation in shapes of the H_2 bands consistent with the model predictions. Generally, auroral spectra tend to show characteristic electron temperatures of 10^6 K or larger. Saturn spectra shown by Shemansky and Ajello [1983] obtained with the Voyager 1 EUV instrument show differences in the 1300-Å region which were not recognized at that time as an effect relating to the exciting electron temperature. The SA model was based on monoenergetic 100 eV electron excitation, which showed a good fit to the auroral data (SA, Figure 3) in the 1250 to 1600-Å region but left an unidentified feature in the equatorial spectrum (SA, Figure 4) near 1330-Å. This feature is now identified as a characteristic of H_2 excited by low-energy electrons at temperatures in the T_e = 10^5 K range [see Ajello et al., 1984, Figure 6]. Figure 7 shows a comparison of a Saturn equatorial spectrum with a strong auroral spectrum, illustrating both optical depth effects and differences in exciting electron temperature. Saturn spectra are chosen in this example because the 1330-Å feature in Jupiter spectra is compromised by high radiation noise levels. The equatorial spectrum in Figure 7 can be modeled with a foreground H_2 abundance $[H_2]\ell \sim 10^{15}$ cm^{-2} and an electron temperature of $T_e \sim 30$ eV, whereas the auroral spectrum requires $[H_2]\ell \sim 10^{20}$ cm^{-2} and electron temperatures of $T_e \geq 100$ eV, with the inclusion of a moderate amount of CH_4 absorption. Figures 8 and 9 show expanded plots of the 800 to 900-Å region in the Jupiter spectra of Figures 3 and 4, indicating consistent differences in the shape of the N-S versus E-W spectra in both the bulge and antibulge regions, that may be interpreted as differences in the abundance of foreground H_2. This is an expected result because line of sight abundances in the E-W map data should be greater than the N-S subsolar point observations. Thus in a general sense the observed H_2 emissions show changes in shape consistent with variations in the free parameters in the present model.

Atomic hydrogen has a large cross section for electron excitation comparable to the total cross section for the H_2 Rydberg bands. Most of the excitation energy goes into the production of the H Ly α line. The concentration of the excitation process into the H (2p) state, as opposed to the distributed (750 to 1670-Å) system of H_2 Rydberg band transitions, tends to produce a very strong 1216-Å emission feature if the abundances of atomic and molecular hydrogen are of the same order in the excitation volume. On the other hand the cross section for the production of the

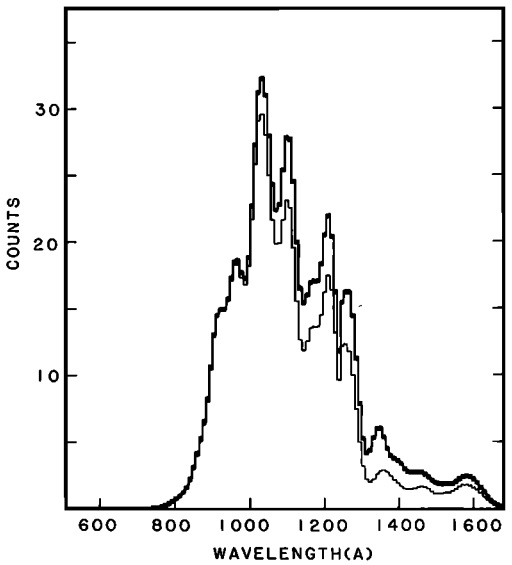

Fig. 6. Model calculations of the H_2 Rydberg system, giving predicted signal for the Voyager 2 UVS instrument. The calculations show the effect of electron temperature on the shape of the emission. The heavy line shows the spectrum at T_e = 2 x 10^5 K; the light line is a spectrum at T_e = 10^7 K. Temperatures above T_e = 10^7 K are difficult to detect. The foreground H_2 abundance in these calculations was fixed at $[H_2]\ell$ = 10^{16} cm^{-2}.

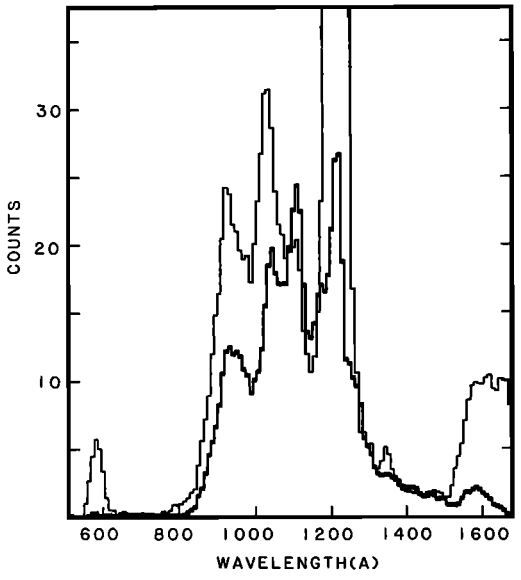

Fig. 7. Voyager 2 spectra of Saturn showing effects predicted by the model calculations. The heavy line is a very bright auroral spectrum in the polar region showing characteristics of large H_2 foreground abundance and high-temperature electron excitation. Deep penetration into the atmosphere is indicated by the shape of the spectrum (800 - 900 Å), a weak relative intensity of the H Ly α line, and the necessity to include a CH_4 absorber in fitting the model to the data. The modeled H_2 and CH_4 abundances are $[H_2]\ell \sim 10^{20}$ cm^{-2} and $[CH_4]\ell = 8 \times 10^{15}$ cm^{-2}. Although the spectrum was taken from the sunlit side, the solar reflection spectrum is absent in the auroral observation because of the high latitude of the source. The light line is an equatorial spectrum very similar to the Jupiter spectra shown in Figures 1 and 2, much higher in the atmosphere ($[H_2]\ell = 3 \times 10^{15}$ cm^{-2}) and showing a sharp peak at ~920-Å characteristic of electron-excited atomic hydrogen. A low temperature for the exciting electrons is indicated by the emission peak near 1350-Å. The equatorial spectrum shows a strong solar reflection spectrum (1500 - 1670 Å), compared to the auroral observations. The spectra are normalized in the 1400- to 1500-Å region.

H Ly α line from dissociative excitation of H_2 is an order of magnitude smaller than that for the e + H process. The low-altitude auroral spectrum shown in Figure 7 is an example of a spectrum dominated by the electron excitation of H_2 in a confined location in the atmosphere, because it shows a very weak 1216-Å line relative to the H_2 bands. The model calculations presented here include the higher Rydberg series lines of atomic hydrogen produced from both direct electron collisions with atomic hydrogen and dissociative excitation. The cross sections of the dissociative excitation process show an approximate n^{-6} dependence on the principal quantum number, n, whereas direct atomic hydrogen excitation (e + H) cross sections show a much more developed $\sim n^{-3}$ dependence. The e + H model in this case is more exact in that the computational method described by Shemansky and Smith [1981] for systems in collisional equilibrium is applied to the H electronic structure. The excitation shape functions for e + H were obtained from theoretical close coupling calculations by Kingston et al. [1976] and Burke et al. [1967]. The selection of these cross sections in preference to experimental results is discussed by Shemansky et al. (unpublished manuscript, 1984). Cross sections for principal quantum numbers $n > 2$ were derived using the collision strength shape functions established for $n = 2$, with absolute values fixed by the Born approximation component. Cross sections for the dissociative excitation process, $n > 2$, were established from the results obtained by Ajello et al. [1984]. Optical depth effects are taken into account directly in the model calculations for emissions arising from levels $n \geq 3$ in which single scattering theory is adequate because of fluorescence losses. However, the H Ly α line does not have a branching loss mechanism, and multiple scattering theory is required to estimate apparent emission rates from an extended source. Calculations on this basis have been addressed by Gladstone [1984], and the theory will be applied in more detail in later work. For present purposes, only rough estimates of expected apparent emission rates will be discussed.

Analysis of the Bulge/Anti Bulge Spectra

The spectra described above and shown in Figures 1 and 2 have been analyzed using models based on the reactions

(R1) $e + H_2(X) \rightarrow H_2 + h\nu(\text{Rydberg}) + e$

(R2) $e + H_2(X) \rightarrow 2H(1s) + h\nu(1s\text{-}n\ell) + e$

(R3) $e + H(1s) \rightarrow H(1s) + h\nu(1s\text{-}n\ell) + e$

(R4) $h\nu + H(1s) \rightarrow H(1s) + h\nu(1s\text{-}n\ell)$

(R5) $h\nu + He(1s^2) \rightarrow He(1s^2) + h\nu(1s^2\text{-}1s2p)$

(R6) $h\nu + H_2(X) \rightarrow H_2^+(X) + e$

(R7) $h\nu + H_2(X) \rightarrow H_2(X) + h\nu(\text{Rydberg})$

given in more detail in Table 1.

The modeled best-fit to the bulge spectrum of Figure 2 is shown in Figure 10. The model contains H_2 Rydberg bands excited at two locations in the atmosphere, a weak component with $[H_2]\ell = 1 \times 10^{18}$ cm^{-2}, and a dominant component at $[H_2]\ell \simeq 10^{15}$ cm^{-2}. The foreground of H_2 in the weak component is an assumed value based on the knowledge that the solar photoelectron component in the emission would be produced mainly at that level. However, the foreground H_2 in the dominant high-altitude component is dictated by the requirement that the model fit the data in the short-wavelength region of the spectrum. The temperature of the exciting electrons in the deeper component is more critical because it tends to control the shape of the spectrum in the 1100 to 1150-Å region; an electron temperature of $T_e = 1.5 \times 10^5$ K provides an optimal fit to the spectrum. The dominant upper component in the model has an electron temperature of $T_e \sim 6 \times 10^5$ K. The temperature of the atmospheric H_2 in the model cal-

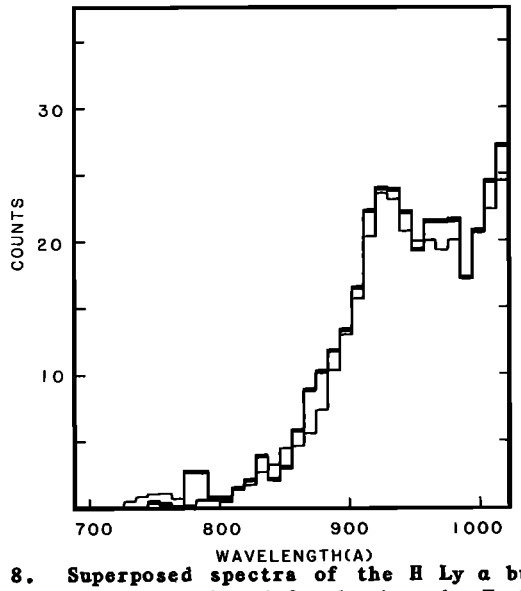

Fig. 8. Superposed spectra of the H Ly α bulge region from Figures 1 and 2, showing the H_2 Rydberg bands in the 700- to 1000-Å region. The heavy line is the N-S map spectrum; the light line is the E-W map spectrum. Although the two spectra have very nearly equal intensities in the H_2 bands, the N-S spectrum shows a different shape in the rising edge of the 800- to 900-Å region indicative of a reduced amount of H_2 foreground gas (see Figure 5) relative to that in the E-W map spectrum. The characteristics of the curvature in the spectra indicate foreground H_2 abundances of ~10^{15} cm^{-2}. See text, and Figure 9.

culation conforms to curve A of Figure 2 of McConnell et al. [1982]. The H_2 temperature is based on an analysis of Voyager occultation by G. R. Smith, and privately communicated to McConnell et al. [1982], who discuss the question of the various estimates. The temperature and density structure is given in Table 2.

The observed spectra in the equatorial region all show a strong peak near 920-Å, whereas the model calculations of the H_2 Rydberg systems never develop a corresponding structure throughout the range of the free parameters (Figures 5, 6). Figure 7 shows a Saturn auroral spectrum in which a 920-Å peak is absent or very weak, and Figure 11 shows deep auroral spectra on Jupiter in which no feature is detectable at this location. The variability among the observed spectra is attributed to variability in the contribution of electron-excited atomic hydrogen, in the set of reactions (R3). The peak at 920-Å is produced by high-order Rydberg transitions in the H structure, limiting at 911.4-Å. The electron-excited component in the spectrum is fitted by varying the amount of H foreground to optimize the shape of the model in the 900 to 1000-Å region (Figure 10). The H Ly β line would normally be the strongest feature for $n > 2$ in (R3) if fluorescent scattering did not remove the line. Higher members of the series approaching 911.4-Å tend toward the optically thin condition because of decreasing transition probabilities as a function of increasing principal quantum number n. The contribution to the spectrum by (R3) is shown in Figure 10. The density of atomic hydrogen involved in (R3) is determined from the modeled high Rydberg members because of the obvious complications involved in the interpretation of the H Ly α feature.

The results of the analysis of the four spectra shown in Figures 1 and 2 are given in Table 3. Those quantities labeled "(source)" are model-inferred rates before absorption or scattering. The details of Table 3 will be discussed later in the text. The salient points derived from the data of Table 3 are given in Table 4 and state that (1) the H Ly α 1216-Å line is enhanced in the bulge by a factor of ~1.4, (2) the electron-excited component of H Ly α 1216-Å (R3') appears to be depressed in the bulge by a factor of 0.75, (3) the He 584-Å line is constant within measurement accuracy, and (4) the H_2 Rydberg bands are constant or slightly depressed in the bulge. Points 1 and 4 are in basic agreement with the conclusions of the earlier work by SBS. The constancy of the He 584-Å line is believed to be established by the present analysis. Point 2 is a result originating with the present analysis, and in combination with points 3 and 4 represents strong observational evidence for the near constancy of the $[H]/[H_2]$ ratio relative to magnetic longitude in the excitation region. Presumably the $[H]/[H_2]$ ratio shows no significant longitudinal dependence at any other altitude in the atmosphere. The electron-excited (e + H) component in fact appears to show a depression in the bulge region. There are three possible explanations for this variation. First, the electron energy distribution of the exciting electrons may change moderately with longitude. Second, minor lowering of the excitation altitude in the bulge region may decrease the $[H]/[H_2]$ ratio for the exciting electrons. A minor softening of the electron spectrum, difficult to detect in this analysis,

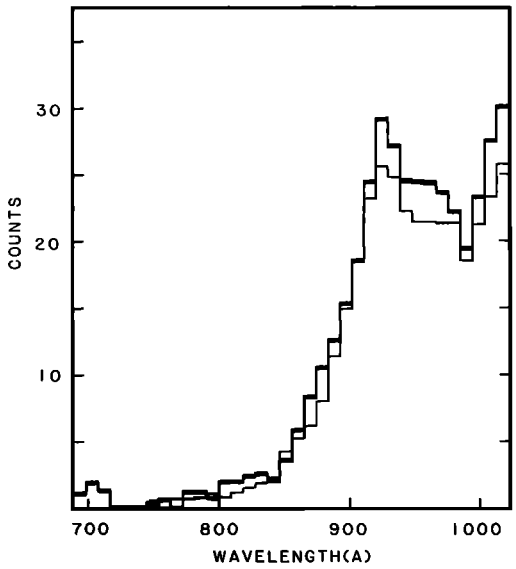

Fig. 9. Superposed spectra of the antibulge region from Figures 1 and 2, counterpart to Figure 8, showing the consistency in shape differences in the 800- to 900-Å region. The implied differences in H_2 foreground abundance are therefore attributed to N-S, E-W geometric factors rather than an effect dependent on magnetic longitude.

would cause an implied decrease in the e + H 1216-Å component that may in fact not be real. A decline in the excitation altitude of ~80 km would produce a similar effect (see Table 2). Third, ambient ionospheric electrons (T_e = 1000 K) and ions may ionize atomic hydrogen in high Rydberg levels. These questions will be discussed in more detail in the following section.

Discussion

The present analysis of the EUV spectra associated with the H Ly α bulge phenomenon introduces two basic constraints that were not available in the earlier published studies. First, a direct measure of the electron-excited component of the atomic hydrogen emission has been obtained as a source quantity. This result indicates that the excitation occurs in the exosphere, and in this interpretation the relative abundance of atomic hydrogen is effectively constant as a function of magnetic longitude. Second, the measured intensity of the solar He 584-Å line scattered by the atmosphere also has no measurable dependence on magnetic longitude. The combined results imply that earlier explanations of the H Ly α bulge phenomenon, all of which depend on a strong longitudinal dependence of relative atomic hydrogen abundance, cannot be supported. Other considerations based on energy deposition characteristics also suggest that a substantial atomic hydrogen bulge is not plausible. These basic conclusions confine the solution to the asymmetric conversion of energy stored within the excited hydrogen system, through control by the properties of the magnetosphere. The exact mechanisms are discussed in detail under the following subheadings. The bulge emission is caused by two processes that occur inseparably in the exosphere, the collisional conversion of H(2s) atoms into the H(2p) state by ionospheric protons and the recombination of H_2^+ and H_3^+ ions with ambient electrons into the excited atomic states. The morphology of the ionosphere controlled by the magnetic anomaly is described here as the basic cause of the emission asymmetry. In this scenario the phenomenon can occur only in the exosphere because of competing reactions at higher densities, and this appears to provide a resonable explanation for the loading of the magnetosphere with H^+, H_2^+, and H_3^+. The variations of the hydrogen emissions over the sunlit disk described here are also consistent with an exospheric source, and in fact a large fraction of the H Ly α emission in this analysis is excited by electrons. However, the importance of the exospheric excitation process to Jupiter's atmosphere lies with the deposition of energy, since the rate of heating may be sufficient to control the temperature from the exosphere down to the hydrocarbon homopause. In addition the process is the dominant source for the upper ionosphere. The ultimate source of energy is left as an unknown in this paper. Solar photons must act as a catalyst, but most of the energy is generated internally. Jupiter's long-term temporal morphology as inferred from Pioneer 10 (P10) and V2 observations is consistent with this conclusion. The results of this work clearly go well beyond the original questions relating to the H Ly α bulge. Apparently the bulge phenomenon is an energetically unimportant outcrop of a process of major

TABLE 1. Reactions in the Atmosphere of Jupiter

Reaction	Rate, 10^{-9} cm^3 s^{-1}	T, K
(R1) $e + H_2(X) \rightarrow H_2(X) + h\nu$(Rydberg) + e	40.	6×10^5
(R2) $e + H_2(X) \rightarrow 2H(1s) + h\nu(1s - n\ell) + e$	4.3	6×10^5
(R2') $e + H_2(X) \rightarrow 2H(1s) + h\nu(1s - 2p) + e$	4.	6×10^5
(R3) $e + H(1s) \rightarrow H(1s) + h\nu(1s - n\ell) + e$	40.	6×10^5
(R3') $e + H(1s) \rightarrow H(1s) + h\nu(1s - 2s) + e$	5.	6×10^5
(R3") $e + H(1s) \rightarrow H(1s) + h\nu(1s - 2p) + e$	31.	6×10^5
(R4a) $h\nu + H(1s) \rightarrow H(1s) + h\nu(1s - 2p)$		
(R4b) $h\nu + H(1s) \rightarrow H(1s) + h\nu(1s - 3p)$		
(R4c) $h\nu + H(1s) \rightarrow H^+ + e$	(7.3×10^8 cm^{-2} s^{-1})	
(R5) $h\nu + He(1s^2) \rightarrow He(1s^2) + h\nu(1s^2 - 1s2p)$		
(R6) $h\nu + H_2(X) \rightarrow H_2^+(X) + e$	(2.6×10^9 cm^{-2} s^{-1})	
(R7) $h\nu + H_2(X) \rightarrow H_2(X) + h\nu$(Rayleigh)	(2 barns at 1216 Å)	
(R8) $e + H(1s) \rightarrow H^+ + 2e$	24.9	6×10^5
(R8') $e + H(10\ell) \rightarrow H^+ + 2e$	4.66×10^3	10^3
(R8") $e + H(20\ell) \rightarrow H^+ + 2e$	1.75×10^5	10^3
(R8"') $e + H(30\ell) \rightarrow H^+ + 2e$	7.3×10^5	10^3
(R9) $e + H_2(X) \rightarrow H_2^+ + 2e$	37.6	6×10^5
(R10) $e + H_2(X) \rightarrow H + H^+ + 2e$	1.9	6×10^5
(R11) $e + H_2^+(1s\sigma_g) \rightarrow H(n\ell) + H^+ + e$	~100.	6×10^5
(R12) $e + H_2^+(1s\sigma_g^2) \rightarrow 2H^+ + 2e$	...	
Recombination		
(R13) $e + H_3^{+*}(X) \rightarrow H(1s) + H(n\ell)$	123.	10^3
(R14) $e + H_3^{+*}(X) \rightarrow H_2(X) + H(n\ell)$	46.	10^3
(R15) $e + H_3^{+*}(X) \rightarrow 3H(1s)$	109.	10^3
(R16) $e + H^+ \rightarrow H(1s) + h\nu$	2.2×10^{-3}	10^3

TABLE 1. (continued)

Reaction	Rate, 10^{-9} cm^3 s^{-1}	T, K
Reactions Involving H(2s)		
(R3''') $e + H(1s) \rightarrow H(2s) + e$	5.	6×10^5
(R2'') $e + H_2(X) \rightarrow H^*(2s) + H^*(n\ell) + e$	3.	6×10^5
(R17) $e + H(2s) \rightarrow H(2p) + e$	4.3×10^4	10^3
(R18a) $H(2s) + H_2(X) \rightarrow H_2(X) + H(2p)$	4.2	10^3
(R18b) $H^*(2s) + H_2(X) \rightarrow H_2(X) + H(2p)$	577.	3.5×10^3, 4.6×10^4
(R19) $H(2s) + E \rightarrow H(2p) + E$	2.8×10^3 E^2(s^{-1})	
(R20) $H(2s) \rightarrow H(1s) + 2h\nu$(cont)	8.23 (s^{-1})	
(R21) $H^+ + H(2s) \rightarrow H(2p) + H^+$	6.5×10^5	10^3
(R13') $H_2^{+*} + e \rightarrow H(2\ell) + H(1s)$	~12.	10^3
(R14') $H_2^{+*} + e \rightarrow H_2 + H(2\ell)$	~10.	10^3
(R22a) $H(2s) + H_2(X) \rightarrow H_3^+ + e$	2.7	10^3
(R22b) $H^*(2s) + H_2(X) \rightarrow H_3^+ + e$	7.0	3.5×10^3, 4.6×10^4
(R11') $e + H_2^{+*} \rightarrow H(2s) + H^+ + e$	~8.	6×10^5
Ion Chemistry		
(R23) $H_2 + H_2^+ \rightarrow H_3^+ + H$	2.	300
(R24) $H^- + H_2^+ \rightarrow H^+ + H_2$	0.58	300
(R25) $H^+ + H_2 + H_2 \rightarrow H_3^+ + H_2$	[3.1 x 10^{-29} cm^6 s^{-1}]	300
(R26) $H^+ + H_2 \rightarrow H_3^+$	...	
(R27) $H^+ + H_2^* \rightarrow H_2^+ + H$	...	
(R28) $H^+ + H(1s) \rightarrow H(1s) + H^+$	60.	10^3
Hydrocarbon Reactions		
(R29) $H + C_2H_4 + [M] \rightarrow C_2H_5$	[9.1 x 10^{-13} cm^3 s^{-1}]	
(R30) $H + CH_3 + M \dashrightarrow CH_4$	[1.2 x 10^{-22}/T^3]	
(R31) $H + C_2H_2 \rightarrow C_2H_3$	[9.2 x 10^{-12} exp(-1210/T)]	

(R1): Calculated from Ajello et al. [1984], Shemansky et al. (unpublished manuscript, 1984) data. (R2, R2'): Excitation function for 2p from Mumma and Zipf [1971], absolute magnitude from Shemansky et al. (unpublished manuscript, 1984), Ajello et al. [1984]. For other nℓ, see Stephens and Dalgarno [1972, 1973], Misakian and Zorn [1972], Leventhal et al. [1967], Vroom and de Heer [1969], Carnahan and Zipf [1977], Freund et al. [1976], Guyon et al. [1979], Julien et al. [1973]. Other references are given by Ajello et al. (1984). (R2''): See (R2), Comes and Wenning [1970]. (R3)-(R3'''): Cross sections from Burke et al. [1967], Kingston et al. [1976], extended to n > 2 with modified Born approximation [Shemansky et al. (unpublished manuscript, 1984)]. Statistical collisional equilibrium calculations as in the work by Shemansky and Smith [1981]. (R4c): Photoionization rate from solar continuum estimated using an adjusted solar source based on the Donnelly and Pope [1973] and Voyager data. (R6): Ionization/neutral dissociation branching calculated from Lee et al. [1976], Dalgarno and Allison [1969]. Solar ionizing flux as measured by Carlson et al. [1984], and scaled data of Donnelly and Pope [1973]. (R7): Heddle [1962]. (R8): From measured cross sections of Kieffer and Dunn [1966] in agreement with theory of Gryzinski [see Bates et al. 1962]. (R8')-(R8'''): From Gryzinski [see Bates et al., 1962]. (R9): From measured cross sections Kieffer and Dunn [1966]. (R10): From measured cross section, Crowe and McConkey [1973]. See Bottcher [1974], Hazi [1975]. (R11): Calculated from measurement [Dance et al., 1967; Dunn and Van Zyl, 1967], theory [Dunn, 1966; Peek and Green, 1969; Peek, 1967]. (R11'): See Peart and Dolder [1974a], text. (R13): Calculated from measurements [Peart and Dolder, 1974a; Auerback et al., 1977]. (R14), (R15): Calculated from measurements [Mitchell et al., 1983]. See also Auerback et al. [1977], Peart and Dolder [1974b], Mathur et al. [1978]. (R16): Theory, Brown and Matthews [1970]. (R17): Theory, Purcell [1952]. (R18a), (R18b), (R19): Calculated from measurement [Comes and Wenning, 1969a]. (R20): See Brown and Matthews [1970]. (R21): Theory, Purcell [1952]. (R22a), (R22b): Calculated from measurement [Comes and Wenning, 1969b]. (R23): First shown to be a rapid reaction through the calculation of Eyring et al. [see Glasstone et al., 1941]. Later laboratory work gave exactly the same rate coefficient [Huntress, 1974]. (R24): Herbst and Klemperer [1973]. (R25): Johnson and Biondi [1974]. (R28): See Newman et al. [1982 and references therein]. (R29), (R30), (R31): Ashihara [1983].

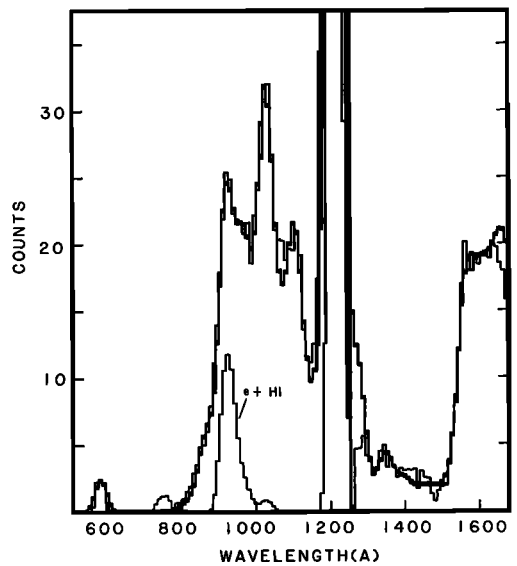

Fig. 10. Model fit to the Jupiter E-W H Ly α bulge spectrum of Figure 2. The heavy line is a model calculation with parameters given in Table 3. The electron-excited atomic hydrogen (e+H) component in the model is shown as a light plotted line with a peak near 920 Å and at 1216 Å. The relative weakness of the H Ly β line at 1025 Å is caused by optical thickness of foreground atomic hydrogen (see text).

importance to the dynamics of the upper atmospheric-magnetospheric system, if the present analysis is correct. Clearly, the implications of these results should be examined further, and the main question concerning internal energy generation must be pursued. A detailed discussion of the main points in this preamble follows under specific subheadings.

The Role of H(2s) Atoms

The observational evidence, if one accepts the analysis presented above, directly precludes a longitudinal variation in the abundance of atomic hydrogen, on Jupiter. There are other indirect arguments, discussed below, relating to the implausibility of a physical process which allows the nonuniform production of atomic hydrogen without producing accompanying effects on the character of the EUV radiation spectrum. Each of the postulations in the earlier work on the subject can be approached quantitatively, although none of the previous authors such as SBS or DSA have addressed the questions in this way. However, the first issue that must be approached here is the question of how one may produce a longitudinal asymmetry in the emission rate of H Ly α in a constant atmosphere of atomic and molecular hydrogen, without producing a similar asymmetry in the electron-excited H_2 Rydberg bands. The thresholds of excitation for the atomic line and the Rydberg bands are separated by only ~2 eV. The solution must then lie within the electronic structure of the hydrogen atom, and/or with a reaction producing H(2s,2p) atoms from H_2^+ or H_3^+ in a variable ionosphere. The discussion below in fact will show that both possibilities are inseparable in producing the observed effect.

We therefore require a mechanism for storage of electronic energy in the H atom which is asymmetric in its release in the atmosphere, and/or a production mechanism such as charge exchange or recombination reactions that produce H(2p) atoms without the involvement of hot electrons. The energy deposited in the hydrogen atom through electron impact excitation is radiated within a 1 μs period for all excited states with the exception of the H(2s) state and the higher Rydberg levels approaching the Rydberg limit. The high Rydberg levels collect only a small fraction of the excitation events and do not contribute measurably to the production of 1216-Å photons either through cascade transitions or radiationless deactivation. However, the H(2s) state is excited at significant rates by several processes as shown in Table 1,

(R3''') $e + H(1s) \rightarrow H(2s) + e$

(R2'') $e + H_2(X) \rightarrow H^*(2s) + H^*(n\ell) + e$

(R14') $H_3^{*+} + e \rightarrow H_2^*(X) + H(2\ell)$

(R13') $H_2^+ + e \rightarrow H^*(2s) + H^*(1s)$

(R11') $H_2^+ + e \rightarrow H^*(2s) + H^{*+} + e$

The rate coefficients for (R3''') and (R2'') are known, but there is uncertainty in the branching of (R13) and (R14), giving the products of (R13') and (R14'). Reaction (R14') is endothermic in the ground vibrational level of H_3^+, and we require vibrational levels of at least (1,0,0), ~0.4 eV above the ground state, for recombination with very low energy electrons. If the combined electron and H_3^+ vibrational energy is above 0.93 eV, the dominant product is (R14'), according to Kulander and Guest [1979]. At lower energies the product species are dominated by H_2X + H(1s) and 3H(1s) [Kulander and Guest, 1979; Mitchell et al., 1983]. The Mitchell et al. [1983] measurements, which represent recombination of H_3^{*+} in an ill-defined vibrational distribution, are reflected in the rates given in Table 1 for (R14) and (R15).

TABLE 2. Jupiter Neutral Atmospheric Temperatures and Densities

T, K	h*, km	$[H_2]$, cm^{-3}	$[H_2]\ell$, cm^{-2}	[H], cm^{-3}	$[H]\ell$, cm^{-2}	$\frac{[H_2]\ell}{[H]\ell}$
803	785	8.2 + 10	1.0 + 18	9.3 + 8	2.1 + 16	476
923	1290	2.1 + 9	3.0 + 16	1.4 + 8	4.0 + 15	75
972	1835	6.2 + 7	1.0 + 15	2.3 + 7	7.4 + 14	1.4

Data are after G. R. Smith [see McConnell et al., 1982].
*altitude above the 1-bar level.

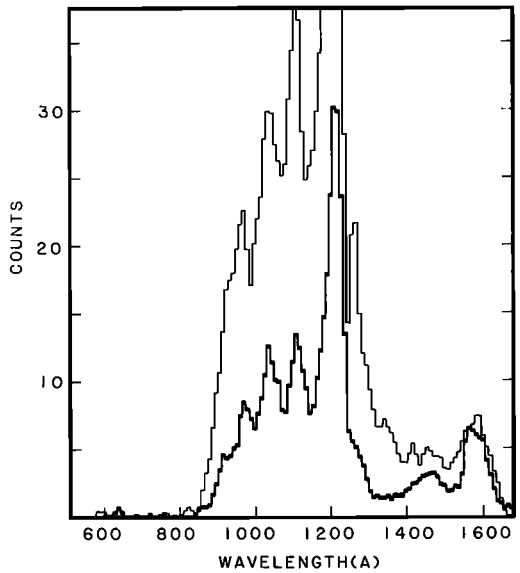

Fig. 11. Voyager 2 spectra of Jupiter aurorae. The heavy line is a darkside spectrum showing strong effects of hydrocarbon absorption, obtained on day 193, 1979, at 2300, at a magnetic longitude of ~270° λ_{III}, in the active sector. The light line is a spectrum from the dayside obtained on day 187, 1979, at 2200, at magnetic longitude of ~100° λ_{III}, in the quiet sector. Both spectra show no sign of an electron-excited atomic hydrogen component; there is no detectable feature at ~920 Å, and the spectra are distinctly different from the equatorial spectra of Figures 1 and 2. The peak at 970 Å is part of the H_2 Rydberg band structure (see Figure 5). The spectra are normalized at 1580 Å, where hydrocarbon absorption is at a minimum. The darkside spectrum is obviously much more strongly affected by foreground hydrocarbon absorption and is substantially deeper, below the hydrocarbon homopause. Primary auroral particles producing the emission must have the equivalent penetration depths of >30-keV electrons.

It is assumed that 50% of (R14') produces H(2s) atoms. The rate coefficient for (R13), which branches to (R13'), is large because the H_2^+ is vibrationally excited, and at electron densities of order [e] ~ 10^5 cm^{-3}, this reaction competes with (R23) at H_2 densities of order 10^7 cm^{-3}, for the removal of H_2^+ ions. Reaction (R13'), the branch of (R13) giving H(2s) atoms as a product, has an uncertain rate. Calculations cited by Peart and Dolder [1974a] suggest a possible branch fraction of 0.05 for (R13'). However, the theoretical calculations produce absolute rates an order of magnitude lower than measurement [Peart and Dolder, 1974a]. Reaction (R11') is not expected to make a significant contribution, because it requires electrons above ~2 eV in order to proceed at a high rate and therefore cannot compete with the recombination process for the removal of H_2^+ ions. The observational fact that the H_2 bands are constant in magnetic longitude, fixes the production of H(2s) atoms through (R3''') and (R2'') as a constant in magnetic longitude, given a constant H and H_2 distribution. The production of H(2s) atoms by (R14'), (R13') and (R11') may show longitudinal variability if Jupiter's ionosphere has structural dependence on magnetic longitude as one may well expect. However, the constancy of the H_2 band emission against magnetic longitude also implies constancy in the production of electron-ion pairs. The ionization source implied by the observed H_2 Rydberg system emissions must completely dominate the production of ionospheric particles in the exobase, as we shall see later in the discussion, and therefore the ionospheric source function must also be constant in magnetic longitude. Any ionospheric properties with a dependence on magnetic longitude must then presumably develop as a result of asymmetry in transport or recombination loss factors. In this regard, the lifetimes of H_3^+ and H_2^+ are in the 100-s to 1000-s range at the altitudes of interest. The production of neutral excited atoms from these ions through (R13') and (R14') will tend to be decoupled from the characteristics of the production of H_2 Rydberg system photons, because rates have a dependence on ambient electron density. In contrast, the recombination lifetime of H^+ (reaction (R16)) is of the order of 50 days or longer, and production through direct electron impact ionization (reaction (R8)) is substantial in the exobase region. Protons are therefore a substantial ionospheric component at virtually any altitude of interest, and in the exosphere the dominant loss process must be transport out of the local volume to reactions elsewhere in the atmospheric-magnetospheric system. Recombination of H^+ into the H(2ℓ) state is negligibly slow and can be neglected as a source, assuming ion densities of order 10^5 cm^{-3}. Given this basic ionospheric condition, dominated by H^+, we must then conclude that the only plausible mechanism within the observational and physical chemistry constraints is a combination of a process of preferential conversion of H(2s) into H(2p) atoms and one of variation in recombination rates of (R13) and (R14) caused by variation in ambient electron density.

The reactions affecting the production and deactivation of H(2s) atoms are shown in Table 1. The contributions of the important source processes estimated from the analysis of the observed spectra are shown in Table 3. The emissions listed in Table 3 labeled as source quantities, as mentioned above, refer to the estimated brightness at the source before inclusion of absorption or multiple scattering processes. The production of H Ly α by electron impact is dominated by direct electron excitation of H(1s) (reaction (R3''), Table 1; sixth row, Table 3). The production of H(2s) atoms by the same process (reaction (R3'''), Table 1; seventeenth row, Table 3) is approximately in the same ratio as the observed variability of the equatorial H Ly α line. However, there are other potentially stronger sources of H(2s) atoms through either of the recombination reactions (R13') or (R14'), giving the possible total production rates shown in the nineteenth row, Table 3. According to Gladstone [1984] an internal atmospheric source of H Ly α over an extended region under optically thick conditions can show a surface brightness as much as four times the brightness of the local optically thin source. Thus in the analysis shown in Table 3, H(2p) atoms excited directly by electrons could contribute as much as 13 kR of the

TABLE 3. Analysis of Mean Longitudinal Asymmetry Spectra of Jupiter

	Bulge E-W	Bulge N-S	Anti bulge E-W	Anti bulge N-S
Emission Intensities, Rayleighs				
H_2 (Ly + Wr) (source)	≥1,730	≥1,880	≥1,920	≥1,970
H_2 (Ly + Wr) (source)	≤976	≤1,060	≤976	≤1,060
H_2 (Ly + Wr) total production	2,710	2,940	2,900	3,030
H I (1s - 2p) 1216 Å; e + H_2X (1) (source)	193	193	217	205
H I (1s - 2p) 1216 Å; e + H_2X (2) (source)	86	103	86	103
H I (1s - 2p) 1216 Å; e + $H I_+$(1s) (source)	2,770	2,480	3,470	3,070
H I (1s - 2p) 1216 Å; e + $(H_3)^*$ (source)	≤ 850	≤ 920	≤ 910	≤ 950
H I (1s - 2p) 1216 Å; residue; solar scatter	(2,000-9,000)	(6,000-14,000)		
H I (1s - 2p) 1216 Å; total observed	17,500	21,700	14,500	15,900
H I (1s - 3p) 1025 Å; e + H_2X (1) (source)	14.4	14.3	16.0	15.2
H I (1s - 3p) 1025 Å; e + H_2X (2) (source)	5.4	6.5	5.4	6.5
H I (1s - 3p) 1025 Å; e + H I (1s)	5.5	4.9	6.9	6.5
H I (1s - 3p) 1025 Å; residue; solar scatter	40.4	40.4	40.4	51.3
H I (1s - 3p) 1025 Å; total observed	66	66	69	79
H I (2s) production; e + H_2X (1)	108	108	121	114
H I (2s) production; e + H_2X (2)	82	98	82	98
H I (2s) production; e + $H I_+$	505	453	632	604
H I (2s) production; e + $(H_3)^*$	≤ 850	≤ 920	≤ 910	≤ 950
H I (2s) production; total rate	≤1,550	≤1,580	≤1,750	≤1,770
He I ($1s^2$-1s2p) 584 Å; solar scatter	4.0	8.2	4.2	9.2
Atmospheric reflection 1600 Å; solar	118(R/Å)	153(R/Å)	122(R/Å)	177(R/Å)
Foreground Abundance, cm^{-2}				
H_2 (1)	$8x10^{14}$	$8x10^{14}$	10^{15}	$8x10^{14}$
H_2 (2)	10^{18}	10^{18}	10^{18}	10^{18}
H I	$6x10^{14}$	$4x10^{14}$	$6x10^{14}$	$4x10^{14}$

See Figures 1 and 2.

observed H Ly α emission, and if all of the H(2s) atoms produced were converted to the H(2p) state we would obtain a possible total of 20 kR, excluding the solar resonance scattered component. On this basis we have a potentially more than sufficient production rate of H(2s) atoms to account for the asymmetry in magnetic longitude provided the prevailing atmospheric condition allows the H(2s) → H(2p) transition with the necessary rate to compete against the other modes of H(2s) deactivation. Variability will in addition be further enhanced through reactions (R13) and (R14) because of variation in the density of ambient electrons with magnetic longitude, as discussed below.

A number of processes can deactivate H(2s) atoms, as shown in Table 1. The ultimate limiting factor in the loss of H(2s) atoms is two-photon radiation [see Osterbrock, 1974], with a lifetime of 0.12 s, and any competing process must therefore show a shorter lifetime in order to defeat radiative loss. The quantities of import required to compete with two-photon continuum loss are given in Table 5. Protons are clearly very effective in producing the H(2s) → H(2p) transition and in the exobase region would very likely be the controlling factor for H(2s) atoms. An excitation process at altitudes below a density level of $[H_2] = 2 \times 10^9$ cm^{-3} would allow prevalence of (R18a) and (R18b) and tend to defeat the development of a magnetic longitude asymmetry. We therefore require the excitation process to proceed primarily in the exosphere. An electric field of at least 54 mV cm^{-1} is required to produce an H(2s) → H(2p) transition in competition with the radiative process. According to A. J. Dessler (private communication, 1983), fields of this magnitude are improbable. A motional ($\vec{V} \times \vec{B}$) electric field of ~15 mV cm^{-1} produced by thermal motion (T = 1000 K) in a $|\vec{B}|$ = 4 gauss field is insufficient to significantly affect the H(2s) lifetime. The most likely reaction to produce an asymmetric emission in H Ly α therefore appears to be (R21), the H(2s) reaction with ambient protons.

TABLE 4. Jupiter Bulge/Antibulge Ratios

Emission Component	Ratio
H I (1216 Å) observed intensity	1.36
H I (1216 Å) e + H I component	0.75
He I (584 Å)	0.90
H_2 Rydberg bands	0.95

Source Altitude and Mechanics of Production and Loss

On the basis of the estimated abundances of foreground H_2 and H gas required by the model fit

TABLE 5. H(2s) Deactivation

	Parameter	Value
Quantities required to compete with two-photon continuum emission	[e], cm^{-3}	2 x 10^5
	[H$^+$], cm^{-3}	1.3 x 10^4
	[H$_2$], cm^{-3}	2. x 10^9
	E, mV cm^{-1}	54
	$(\vec{V}\times\vec{B})^*$, mV cm^{-1}	~15

*Motional electric field at T = 1000 K.

to the data shown in Table 3, the upper emission source region is located at altitudes where [H_2] ≈ 6 x 10^7 cm^{-3} and [H] ≈ 1.6 x 10^7 cm^{-3} with abundance ratios [H_2]ℓ/[H]ℓ ranging from 1.3 to 2. This result is consistent with the Voyager occultation data shown in Table 2, in the sense that the estimated H_2 and H densities obtained from the model analysis correspond to the same altitude, ~1800 km above the 1-bar level. A further independent measure of [H_2]ℓ/[H]ℓ can be obtained from the relative intensities of the modeled H_2 and H emission rates at the source (Table 3), and the known excitation rate coefficients. The ratio [H_2]ℓ/[H]ℓ ≈ 0.6 obtained with the latter method is as much as a factor of 3 below the estimate obtained from the self-absorption measures. This difference reflects the uncertainties in the analysis, such as relative amounts of high- and low-altitude components in the H_2 Rydberg bands, the effective temperature of the exciting electrons, and statistical uncertainty of the spectral profile in the short-wavelength regions critical to the optical depth estimates. A moderately lower electron temperature in the high-altitude component, for example, would tend to bring the two sets of [H_2]ℓ/[H]ℓ ratios into better agreement. However, we note from Table 2 that the very strong dependence of the [H_2]ℓ/[H]ℓ ratio on altitude and the values calculated by the two methods place the high-altitude source in the 1800- to 2100-km range. A moderate systematic difference in respect to magnetic longitude appears in the electron-excited high Rydberg lines of atomic hydrogen (Tables 3, 4). There are a number of possible explanations. For example, the effect could be produced by a moderate change in excitation altitude. Assuming a constant electron temperature, one would infer the altitude of the antibulge emission to be higher by about 80 km relative to the electron excited bulge emission. Over this altitude range, H_2 densities vary by a factor of 1.6, and yet the H_2 Rydberg systems remain constant in intensity within ~5% (Table 4). If a systematic variation in excitation altitude does in fact occur, it is remarkable that electron densities and/or temperatures adjust to maintain near-constant radiative energy production. In fact this chacteristic may argue against variation in the source altitude as an explanation of the variation in implied H_2/H electron excitation rates. One could alternatively invoke a moderate 20% variation in the [H_2]/[H] ratio in the exobase with the antibulge region containing a relatively greater abundance of atomic hydrogen. However, a physical argument for the latter condition is not clear in the face of constancy in the excitation of the H_2 Rydberg systems. The most likely explanation for the variation in implied H_2/H excitation rates lies in electron and proton deactivation of the high Rydberg H(nℓ) levels because these levels provide our measure of the e + H component in this analysis. If ionospheric densities are substantially different in the excitation regions of the H Ly α bulge/antibulge longitudes, as suggested below with a maximum in the bulge region, we may then have a variation in radiationless deactivation of the H(n > 15) states by ambient ions and electrons through processes of ionization and angular momentum transitions. The electron ionization rates for high Rydberg levels are shown in Table 1, (R8'), (R8''), (R8'''). Atoms in the n = 30 states are lost to ionization by electrons at [e] = 2 x 10^5 cm^{-3} density at rates comparable to the radiative lifetime. A more detailed calculation than that provided in the present paper is required to establish the magnitude of the effect on the aggregate of levels contributing to the observed emission, but it appears that radiationless deactivation of H(n > 15) by ionospheric particles could possibly account for the observed bulge/antibulge variation. If this explanation is correct, the estimated direct electron excitation contributions to H Ly α emissions given in the sixth row of Table 3 would tend toward constancy in respect to bulge/antibulge magnetic longitudes. The estimated emission altitude of the particle-excited components lies in the region of substantial ionospheric densities, according to the direct measurements by the Voyager radio science experiments [see McConnell et al., 1982]. The estimated peak electron densities can be as high as [e] = 2 x 10^5 cm^{-3} at 1600- to 2300-km altitudes. It is difficult to obtain a well-defined morphology of the ionosphere because the occultations by both Pioneer and Voyager spacecraft occurred at different latitudes, with probable varying degrees of involvement with auroral activity. However, assuming that a large fraction of the ionospheric ions were H^+, one would expect the H(2s) → H(2p) process to proceed over a substantial fraction of the period, and we would require H^+ densities of 10^4 cm^{-3} or lower in order not to perturb the H(2s) population. Thus, if for some reason the H^+ densities at the production altitudes of H(2s) atoms were dependent on magnetic longitude, all of the quantitative conditions for producing the observed variation in H Ly α emission would be obtained. A complicating factor in considering the interaction of the ionospheric H^+ with the H(2s) atoms produced by the electron excitation process, is that the H^+ ions must ultimately be produced by the same energetic electrons. The mechanics of the reaction regime producing the H Ly α bulge therefore tends to be self-limiting. Figure 12 shows the production efficiencies of dissociated hydrogen, H_2^+, and direct and indirect excitation of H_2 Lyman and Werner bands, as a function of the temperature of the exciting electrons. At electron temperatures T_e > 2 x 10^5 K the production of H_2 Lyman and Werner band photons has about the same efficiency as that of neutral atoms and H_2^+. The major branches of H_2^+ chemistry end in neutral atoms, as discussed above, and a substantial fraction of the ion production arises in direct ionization of atomic hydrogen. The efficiency for direct electron ionization of H is similar to that for H_2. The H^+ production rate in the vicinity of 1800 km is

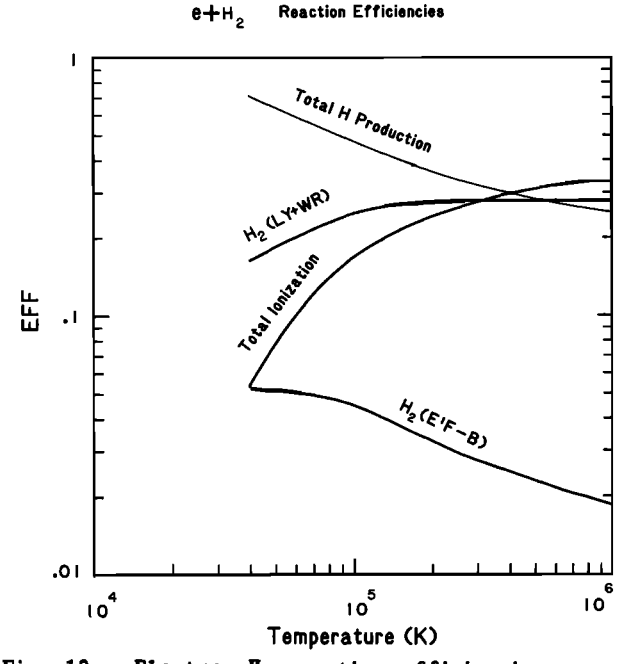

Fig. 12. Electron-H_2 reaction efficiencies, as a function of electron temperature. Neutral dissociation rates were obtained from cross sections compiled by D. E. Shemansky and G. R. Smith (manuscript in preparation, 1984). The curve marked H_2 (Ly+Wr) is the efficiency of photon production in the Lyman and Werner bands, exclusive of the E,F-B cascade component, calculated from Ajello et al. [1987] data. The curve marked H_2 (E,F-B) is the cascade component contribution to the H Lyman band emission. The curve marked Total Ionization is calculated from data cited in Table 1. The efficiencies are calculated relative to the total inelastic cross section.

therefore ~ 2.7 x 10^9 cm^{-2} s^{-1}. In order to maintain an ionospheric density $10^4 \leq [e] \leq 2 \times 10^5$ cm^{-3} we require an H^+ residence lifetime in this region of 200 s to 3500 s, implying transport loss velocities of > 80 m s^{-1}. If the H Ly α bulge is caused by variation in local ionospheric proton density as suggested here, then we appear to require a variation in transport loss to control the ion population. If this is the case, then, as discussed below, H_3^+ and H_2^+ may also play a role in the production of the H Ly α bulge through a variable recombination rate. In order to produce the observed electron excitation we require a relatively constant density [e] in the range ~20-160 cm^{-3} of hot (T_e ~ 6 x 10^5 K) electrons immersed in the variable ambient electron population.

Variation Over the Sunlit Disk

A remarkable aspect in the comparison of the E-W and N-S map data is the constancy of the H_2 Rydberg band brightness. The E-W map observations represent averages over local solar phase, whereas the N-S data contain emissions from the region of the subsolar point. Therefore any source having limb-darkening effects will show a lower brightness in the E-W map data. The strongest effect is in the He 584-Å line, in which the N-S/E-W brightness ratio is 2 (Table 3). The H Ly α line shows a value N-S/E-W ~ 1.2, while the H_2 Rydberg bands remain constant. The variations in the major emissions across the sunlit face of Jupiter are shown in Figure 13, averaged over magnetic longitude in the E-W map data. The H_2 Rydberg bands show a monotonic rise in brightness between the dawn and dusk limbs with the exception of the region close to the dawn limb. The total H Ly α emission shows a tendency to follow the H_2 emission between -0.4 R_J and +0.6 R_J with a limb-darkening effect on either side. The He 584-Å line shows pronounced limb darkening and possibly some structure, although it is not certain that all of the structure is real. The solar reflection spectrum also shows limb darkening (see also Clarke et al. [1982]), intermediate between that of the H Ly α and He 584-Å lines. The H_2 Rydberg bands have the characteristic of an optically thin solar controlled shell, but for the fact that there is no apparent limb brightening [Gladstone and Shemansky, 1983]. No attempt will be made in this paper to model the dawn-dusk characteristics of the longitudinally averaged data, but the distributions are described here to point out the tendency of H Ly α dawn to dusk

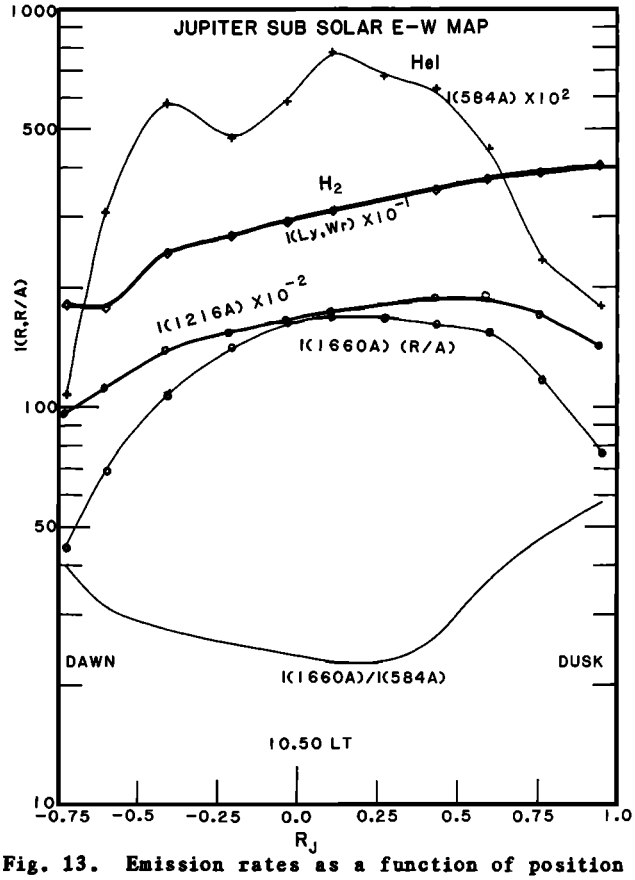

Fig. 13. Emission rates as a function of position along the equatorial belt of Jupiter obtained from Voyager 2 E-W map data averaged over all magnetic longitudes. The data are obtained through model analysis similar to that shown in Figure 10 and Table 3. The curvature shown in the H_2 (Ly+Wr) emisison plot at -0.75 to -0.4 R_J is considered to be real, but the fine structure in the He (584 Å) curve may be statistical in nature.

distribution to follow that of the H_2 Rydberg systems over a substantial fraction of the disk. This is interpreted here as a further confirmation of the model analysis shown in Table 3 indicating that at least 1/2 of the observed H Ly α emission is produced internally by electron excitation. An electron-excited H Ly α emission of this magnitude relative to that of the H_2 Rydberg bands can only be produced in the exobase region as discussed above, where the relative population of atomic hydrogen is sufficiently large.

Morphology of the Bulge

Acuña and Ness [1976] describe an asymmetric locus of the charged particle magnetic equator on Jupiter through the trace of the minimum in the magnetic field intensity. Dessler and Vasyliunas [1979] have developed a magnetic anomaly model based on the asymmetry in the field, designed to explain periodicities in magnetospheric phenomena. The latter authors described a region surrounding $\lambda_{III} = 230^0$ as the active sector in which magnetospheric plasma tends to be lost through precipitation and scattering in the atmosphere promoted by lowered mirror points in a region of weakened magnetic field. The active sector is therefore a region of depleted plasma, whereas the magnetic longitudes in opposition forming the quiet sector tend to contain relatively higher plasma densities because of significantly lower transport or convective losses. The bulge region in H Ly α emission described by the data analysis presented by DSA corresponds roughly to the quiet sector region. Moreover, DSA show an important result indicating the trace of the H Ly α isophote contours to be in conformation with the charged particle drift equator as described by Acuña and Ness. This result therefore strongly suggests that the H Ly α bulge conforms to the regions of maximum plasma density. If we assume, as discussed above, that the ionospheric density is controlled by transport properties and that vibrationally excited H_2 does not play a strong role in removing H^+ (reaction (R27), Table 1 [cf. McConnell et al., 1982]), then one can obtain the basic condition required to produce the H Ly α bulge. The modification of transport loss by the magnetic anomaly, producing a variation in ambient density as a function of magnetic longitude, will then produce the H Ly α bulge under a condition of longitudinally invariant ion production rates. We can select an example of excitation-ionization collisional equilibrium at 1800 km (Table 2) to show the effect on H Ly α emission rates of an ionosphere controlled by transport loss, in a roughly simplified manner. Time constants, as discussed above, appear to be short enough that steady state equations are applicable over most of the dayside atmosphere. Protons are controlled by transport loss, so that one can relate production of H^+ (P_+) to a transport loss probability

$$D = P_+/[H^+] \quad s^{-1} \qquad (1)$$

At this altitude (1800 km), H_2^+ is rapidly converted to H_3^+ (reaction (R23), Table 1) and does not play a significant role in the partitioning of ions. The H_3^+ population is controlled by recombination and transport loss (D), and we can write

$$[H_3^+] = P_{3+}/([e](k_{14} + k_{15}) + D) \ cm^{-3} \qquad (2)$$

assuming that both ions are controlled by the same transport property, where P_{3+} is the production rate of H_3^+ and $k = k_{14} + k_{15}$ is the total H_3^+ recombination rate coefficient. The combination of these equations with charge neutrality then relates electron and ion densities,

$$[e] = \frac{1}{2k}\left[((P_+/H^+)^2 + 2k(P_+ + 2P_{3+}) + [H^+]^2k^2)^{1/2} + [H^+]k - P_+/[H^+]\right] \ cm^{-3} \qquad (3)$$

The production rates P_+ and P_{3+} are fixed by the data analysis at $P_+ = 56\ cm^{-3}\ s^{-1}$ and $P_{3+} = 200\ cm^{-3}\ s^{-1}$. The rate coefficient $k = 1.5 \times 10^{-7}\ cm^3\ s^{-1}$ at $T_e = 1000$ K. Given these quantities, the partitioning of the ionospheric particles is given in Figure 14 for various ambient electron densities through equation (3). At low electron densities $[e] \approx 3 \times 10^4\ cm^{-3}$ caused in this scenario by strong transport loss in the active sector, H_3^+ is 2/3 of the total ion population and $[H^+] = 1 \times 10^4\ cm^{-3}$. At high electron densities $[e] = 2 \times 10^5\ cm^{-3}$, say, corresponding to a quiet sector region, H^+ is the dominant ion. Two effects would obtain in relation to H Ly α production betwen the regions of low and high ionospheric densities. First, the increased H^+ density in the high-density region would control the lifetime of the H(2s) population through conversion to H(2p) atoms, as discussed above. Second, the production of H(2ℓ) atoms through H_3^+ recombination (reaction (R14')) increases from low to high ion densities by about a factor of 2. We note, however, that the rate of (R14) will have a complex dependence on electron energy distribution. Although the H_3^+ share in ion partitioning declines rapidly as the electron density increases, the production quotient $[e][H_3^+]$ increases with increasing electron density toward an asymptotic limit (Figure 14). The H Ly α bulge in this system may therefore be produced partially through variation in H(2s) → H(2p) collisional transfer and partially through variation in H_3^+ recombination production rates of H(2ℓ) atoms. The process of H_3^+ recombination variability in magnetic longitude of course represents variation in the production of atomic hydrogen. However, direct electron dissociation of H_2 forms a substantial part of the production of atomic hydrogen (D. E. Shemansky and G. R. Smith, manuscript in preparation, 1984) and one would not expect more than a few percent variation in the longitudinal abundance distribution. The required transport loss time constant for the ions is also shown in Figure 14 and indicates lifetimes ranging from $\tau_D = 1/D = 0.05$ hour for $[e] = 3 \times 10^4\ cm^{-3}$ to $\tau_D = 1$ hour for $[e] = 2 \times 10^5\ cm^{-3}$. The corresponding transport velocities for the ions range from 560 m s^{-1} to 85 m s^{-1}. The calculations discussed here are clearly very rough, and we require detailed model calculations to establish a better understanding of the dynamics of the ionosphere and its role in controlling the particle-excited atomic hydrogen emission from the exosphere. But all of the quantities involved with the production of an H Ly α bulge in the quiet sector through the suggested reactions appear to have the magnitudes required to reproduce the observations. Among the four radio science occultations at Jupiter, shared between

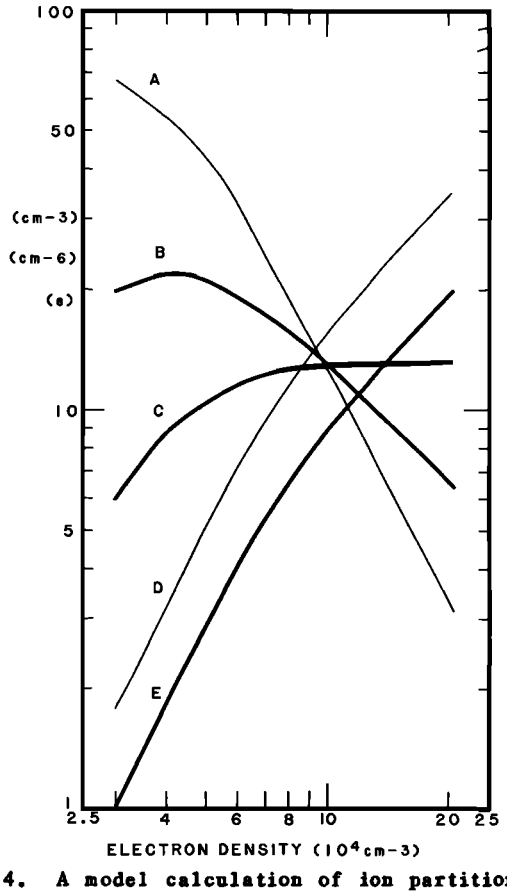

Fig. 14. A model calculation of ion partitioning at 1800 km in the Jupiter ionosphere, as a function of electron density. The calculation assumes a constant source function located within the reaction volume, with recombination and transport as controlling factors in the loss process, as discussed in the text. The production rate of atomic hydrogen, proportional to $[e][H_2^+]$, curve C shown in the figure, increases monotonically with electron density, although the $[H_3^+]$ component, curve B, rapidly declines as shown by the variation of $[H_3^+]/[e]$, curve A. The ion lifetime against diffusive loss (τ_D) from the volume is curve D. The proton density $[H^+]$ is curve E. Values are as follows: (curve A) $([H_3^+]/[e])$, 10^2; (curve B) $[H_3^+]$, 10^3 cm^{-3}; (curve c) $[e][H_2^+]$, 10^8 cm^{-6}; (curve D) τ_D 10^2 s; and (curve E) $[H^+]$, 10^4 cm^{-3}.

the Pioneer and Voyager spacecraft, only Voyager 1 obtained results close to the equator. The other three occultations probably are complicated by auroral activity at higher latitudes [see McConnell et al., 1982]. The Pioneer data are compromised by instrumental difficulties. However, a consistency that does appear among the Voyager occultations is that high electron densities at high altitude (1600 km to 2300 km) are obtained in the vicinity of quiet sector magnetic longitudes. That is, the dawn occultation for Voyager 2 and the dusk occultation for Voyager 1 both show high-density ($[e] \sim 2 \times 10^5$ cm^{-3}) ionospheres, in the quiet sector region. Conversely the dusk occultation for Voyager 2 and the dawn occultation for Voyager 1 show low-density ($[e] \sim 1 \times 10^4$) ionospheres, in the 1600- to 2300-km active sector region. The Voyager radio science occultations are therefore consistent with an ionospheric density structure in magnetic longitude, required for the proposed H Ly α bulge mechanism.

Other Observational Evidence

In general, H_2^+ and H_3^+ are short-lived species. Recombination rate coefficients are very high, of order 10^{-7} cm^3 s^{-1} (reactions (R13)-(R15)), and the reaction of H_2^+ with H_2 is sufficient to effectively convert H_2^+ into H_3^+ (reaction (R23)) even at the altitude of the exobase. In spite of this fact, Hamilton et al. [1980, 1981] have observed substantial abundances of H_2^+ and H_3^+ energetic particles in the range 0.1 - 1 MeV/nucleon throughout Jupiter's magnetosphere. The implication seems to be that reasonably low energy electrons, $T_e = 6 \times 10^5$ K, say, must be involved in the production of H_2^+ at altitudes at least two scale heights above the exobase, either in the auroral zones or at lower latitudes. Voyager observations of sunlit and darkside aurorae shown in Figure 11 both show penetration into and below the hydrocarbon homopause with no easily measurable e + H component, suggesting that energetic particles are responsible for most of the aurora. If these spectra are assumed to be typical, auroral particles would therefore not be efficient in the production of ionization at high altitudes. This raises the possibility that the high-altitude deposition observed in the equatorial region is primarily responsible for the H_2^+ and H_3^+ discovered in the outer magnetosphere by the Voyager low-energy charged particle (LECP) experimenters.

A crude estimate of source and loss rates can be made on the basis of the Voyager LECP and ultraviolet spectrometer (UVS) data. High-altitude H_2^+ produced by primary auroral particles penetrating to the hydrocarbon homopause requires the equivalent of $\gtrsim$ 30-keV electrons [see Yung et al., 1982; Clarke et al., 1980b]. On the basis of a total auroral energy input rate by primary particles of 3×10^{13} W [Broadfoot et al., 1981], 30-keV electrons would produce a globally averaged source rate of H_2^+ of $\sim 1.6 \times 10^{-3}$ ions cm^{-3} s^{-1} in the exobase. The data given here indicate there are $\sim 3 \times 10^9$ H_2^+ ions cm^{-2} s^{-1} produced in the dayside exosphere, averaged from dawn to dusk at the equator. Globally averaged, the dayside airglow produces ~70 H_2^+ ions cm^{-3} s^{-1}, 4 - 5 orders of magnitude larger than the assumed auroral source. The total production rate by the equatorial process in the exobase is

$$P_{2+} \cdot V \approx 7 \times 10^{29} \ H_2^+ \text{ ions s}^{-1}$$

The rate given in the previous section for the production of H^+ is 19 ions cm^{-3} s^{-1}, with a total production rate of

$$P_{+} \cdot V \sim 4 \times 10^{29} \ H^+ \text{ ions s}^{-1}$$

comparable to the H_2^+ value. Hamilton et al. [1983] discuss loss rates of H_2^+ and H_3^+ in the magnetospheres of Saturn and Jupiter. The limiting factor for magnetospheric H_2^+ lifetime at Jupiter is photodissociation [Hamilton et al., 1983], with a maximum value $\tau_r = 60$ days. If we take the mean plasma density in the outer magne-

tosphere as [e] = 3 x 10^{-3} cm^{-3} at Jupiter and calculate a volume on the basis of an 80-R_J radius we have a total of ~2 x 10^{34} electrons. Hamilton et al. [1980] estimate

$$[H_3^+]/[H^+] \approx [H_2^+]/[H^+] = 3 \times 10^{-3}$$

at Jupiter, so that

$$[H_3^+] \cdot V \approx [H_2^+] \cdot V \approx 6 \times 10^{31}$$

assuming that the abundance ratio is constant at all energies. A τ_r = 60 days residence time gives a loss rate of

$$P_{x+} \cdot V = 6 \times 10^{31}/5.2 \times 10^{6} = 1.2 \times 10^{25} \text{ ions } s^{-1}$$

We then require an efficiency of

$$\epsilon = 1.2 \times 10^{25}/7 \times 10^{29} \approx 2 \times 10^{-5}$$

for the transport of H_2^+ ions into the magnetotail from the exospheric source, in order to populate the magnetosphere with energetic ions. However, this efficiency relates to the total production of H_2^+, and only a small fraction of the product is available for transport. About 10% of the H_2^+ production process is in the only vibrational partition (v = 0) available for leakage into the magnetotail because of higher recombination rates for the higher quantum levels [see Hamilton et al., 1983]. Thus very crudely, we may have a maximum leakage efficiency of order 10^{-3} for the available H_2^+ into the magnetotail and ultimately into the magnetosphere as a whole in the form of energetic ions. If this same efficiency applies to H^+, the more stable ionospheric particle,

$$4 \times 10^{26} \quad H^+ \text{ ions } s^{-1}$$

will enter the magnetosphere, implying a

$$\tau_r = 2 \times 10^{34}/4 \times 10^{26} \sim 600 \text{ days}$$

lifetime for H^+. Thus on the basis of these order of magnitude estimates the exospheric equatorial processes on both Jupiter and Saturn appear to be the major source of magnetospheric H^+, H_2^+, and H_3^+. Hamilton et al. [1983] draw the same conclusion, at least for H_2^+ and H_3^+ on the basis of L dependence of phase space distribution, and relative composition.

Energy Deposition

A rough estimate of energy deposition efficiency for electrons at a temperature T_e ~ 6 x 10^5 K using the calculations shown in Figure 12 and using approximate energy loss factors gives a ratio of total energy deposited to that emitted in H_2 Lyman and Werner bands of 4.5. This factor refers to deposition in undiluted H_2. The exospheric composition considered here contains comparable amounts of H and H_2, and therefore a factor for energy loss to the ionization and excitation of H must be included. The estimated energy deposition rate at the subsolar point, based on a 2.2-kR H_2 Lyman and Werner band brightness from the exospheric source, is 0.32 erg cm^{-2} s^{-1}. The deposition of solar energy in the form of photoionization based on the near solar maximum data of Carlson et al. [1984], is 0.077 ergs cm^{-2} s^{-1} for a solar flux of 5.7 x 10^{10} ph cm^{-2} s^{-1} at 1 AU below 575-Å. Most of the energy deposition represented by the observed equatorial emission must then be generated by a mechanism internal to the Jupiter system.

Dayside/Darkside Characteristics, Long Term Temporal Morphology, and the Energy Source for the Exospheric Phenomenon

The electron-excited H_2 Rydberg bands are confined to the sunlit hemisphere, strongly suggesting that solar photons play a controlling role, although they cannot account for the altitude or the energy involved in the exospheric deposition. The characteristic time for the decay of H_2 emissions across the dusk terminator must be short, ~0.5 hour, say, because the Lyman and Werner band intensities fall below 500 R and are undetectable in the dark atmosphere [McConnell et al., 1980]. The only detectable emission on the darkside, H Ly α, shows evidence of a bulge effect according to McConnell et al., 1980]. The latter work suggests that H Ly α is more intense than can be accounted for by scattering of the interstellar-interplanetary H Ly α source, and it was proposed that additional excitation was caused by particle precipitation. If 400- to 600-R of H Ly α emission on the darkside were electron excited with a similar I(H Ly α)/I(H_2 Lyman + Werner) $\simeq$ 3 ratio to that from the sunlit atmosphere, we expect 150- to 200-R H_2 Lyman and Werner band intensities, well below the observational upper limit. However, recombination of exospheric H_3^+ and H_2^+ with ambient electrons in the 2000 km altitude region would certainly continue into the darkside, and on this basis the density of required darkside hot electrons may be even lower or nonexistent if most of the excess H Ly α is generated by recombination.

Although the darkside emission characteristics on Jupiter pose no particular difficulty for the present explanation of the H Ly α asymmetry, the larger question of how the energy deposition implied by the H_2 emissions is derived remains basically unanswered. Saturn shows an essentially similar characteristic with subsolar exospheric energy deposition apparently accounting for the upper atmospheric temperature [Smith et al., 1983; D. E. Shemansky and G. R. Smith, manuscript in preparation, 1984], and no detectable particle excitation in the darkside antisolar region. Saturn has no H Ly α longitudinal asymmetry presumably because the magnetic field is essentially a dipole aligned with the rotational axis. Titan also displays a similar phenomenon with relatively strong exospheric particle excitation of N_2 on the dayside with no measurable continuation across the terminator [Broadfoot et al., 1981; Strobel and Shemansky, 1982]. The relationship between the three planetary bodies relative to the common general exospheric excitation characteristics is obscure. Magnetospheric configurations are certainly different, and it is not at all clear that some common or universal energy injection mechanism applies to all three phenomenologically similar processes. Low-energy solar photons (λ < 912 Å) can produce low-energy elec-

TABLE 6. Measured Jupiter Emission Rates at Pioneer 10 and Voyager 2 Encounters

Pioneer 10	Voyager
Jupiter Encounter	
UV photometer [~400 Å to 750 Å], [~400 Å to 1400 Å] Dec. 1973 solar minimum	UV spectrometer 700 Å to 1700 Å March, July 1979 solar maximum
Dayside Emission	
H Ly α 1216 Å 1.8 kR*	H Ly α 1216 Å 15 kR*
H_2 bands ?	H_2 bands 3 kR
Aurora	
	H Ly α 1216 Å 40 kR
?	H_2 bands 80 kR

*Disk average including both polar regions. The P10 brightness is not corrected for inclusion of H_2 band emission (see text).

trons at high altitudes, but the question of how this weak ionization process may stimulate a process with substantial controlling influence on the upper atmosphere has no apparent resolution. A strong influence of electric fields appears not to be a likely solution especially on Jupiter, because Druyvesteyn electrons in an ionosphere that shows strong density variations would tend to produce variable excitation rates of the electron-excited components. If Druyvesteyn electrons were involved in the excitation, one would require some natural limiting process involving field strength and collisional mean free path variations in order to compensate for ionospheric density variations in maintaining a constant excitation rate. In Jupiter's atmosphere we apparently require a dual population of electrons with $[e_c] \sim 10^4 - 10^5$ cm^{-3}, $T_{ec} < 10^4$ K and a hot population with $[e_h] \sim 30$ cm^{-3}, $T_{eh} \sim 6 \times 10^5$ K at about 1800 km altitude. If the excitation altitude is constant, then $[e_h]$ must be constant against a strongly variable $[e_c]$. Small variations in altitude can be tolerated by the observations, although there is no measurable evidence for a variation. As noted earlier, the uncertainty in the foreground abundance of gas estimated in the analysis may be as large as a factor of 2 or 3. However, although (as shown in Figures 8 and 9) the N-S/E-W spectra show small consistent foreground differences, there is no indication in the data of bulge/antibulge differences (Table 3) in the abundance of foreground H_2. The extent in altitude of the excitation process is not well limited by the observations. It has been assumed in most of the discussion here that the process is confined approximately to one scale height in depth. This may not necessarily be the case if we see no particular limb brightening effects in the H_2 bands (Figure 13), and if the Voyager LECP experiment [Hamilton et al., 1980, 1981] has observed substantial amounts of both H_2^+ and H_3^+ in the outer magnetosphere. The phenomenon of strong exospheric particle excitation in the sunlit atmospheres of Jupiter, Saturn, and Titan is certainly of compelling importance to the understanding of the outer planetary systems, but at this point the author can only indicate some constraining factors in approaching the very obscure solution.

Recent work in obtaining a cross-calibration of the Pioneer 10 (P10) and Voyager EUV instruments (D. E. Shemansky et al., manuscript in preparation, 1984) has produced a measure of the brightness of Jupiter's sunlit hemisphere near the time of solar minimum in 1973/1974 and near the maximum in the 11-year solar cycle in 1979. The apparent brightness of the H Ly α line in the P10 observations must be multiplied by a factor of 4.4 (D. E. Shemansky et al., manuscript in preparation, 1984) in order to place the two instruments on the same calibration standard. The relevant corrected data for the Jupiter observations are shown in Table 6. The deduced H Ly α emission rate (1.8 kR) in December 1973 was an order of magnitude below the rate in 1979. This drastically reduced intensity near solar minimum is supported by rocket and satellite measurements in the interim (Atreya et al. [1982]; however see Skinner et al. [1983]). The P10 instrument is a photometer with rapidly increasing sensitivity at wavelengths shortward of 1216-Å. The assumed H Ly α brightness given here for P10 (1.8 kR) is therefore an upper limit because the signal includes the integrated emission of the H_2 Rydberg bands in the equatorial and auroral zones. Thus over a period in which the solar flux at 1216-Å and shortward may vary by a factor of ~3, the emissions from the dayside face of Jupiter varied by a factor of 10 or more in intensity. Once quantitative limits are set by modeling the H_2 Rydberg bands through the P10 instrument, the implied variation in H_2 emission rates over the half cycle will certainly be larger than a factor of 10. If we make the assumption that the activ-

ity on Jupiter is directly related to solar EUV photon input, the behavior over the half solar cycle again suggests the planet acts as an energy amplifier to solar stimulus, generating substantially more in heat and radiation than solar deposition provides. If the mechanism for the production of the H Ly α bulge follows the description given here, the period of solar minimum is apparently a period of depeleted ion densities in the exosphere to the extent that the phenomenon would no longer be measurable.

Earlier Explanations of the H Ly α Bulge

The initial attempts to explain the H Ly α bulge phenomenon (SBS, DSA) were based on the assumption that the process was a matter of solar resonance-scattered radiation in an atmosphere containing an abundance of atomic hydrogen varying by as much as a factor of 3 as a function of magnetic longitude [McConnell et al., 1981]. Apart from the direct observational constraints placed by the present analysis, the major problem posed by a bulge in atomic hydrogen is that energy is required to produce the dissociated state. The required deposition of energy must in some manner not be shared by the electron-excited H_2 Rydberg bands. The explanation favored by DSA was to introduce relatively high energy particles which penetrate below the hydrocarbon homopause and by that means mask the EUV radiation from the observer. Assuming that the exospheric excitation process is sufficient to maintain the mean abundance of atomic hydrogen on Jupiter, as the same process does for Saturn [Smith et al., 1983], we would require possibly 10 times the exospheric energy deposition rate in the quiet sector to maintain the proposed bulge in atomic hydrogen because of increased lateral diffusion. Furthermore, the dissociated hydrogen must diffuse upward through the hydrocarbons to populate the upper atmosphere. Hydrocarbon chemistry (reactions (R29)-(R31), Table 1) would limit the atomic hydrogen lifetime to ~1000 s in the lower regions, and we require more energy to overcome losses. On this basis we may easily expect a requirement of order ~10 ergs cm^{-2} s^{-1} to maintain the proposed atomic hydrogen bulge. In these circumstances such a process should be observable in hydrocarbon infrared emissions and possibly seriously alter atmospheric composition and structure in the hydrocarbon region. Apart from an objection on the basis of the amount of required energy, the energy spectrum of the exciting particles cannot be expected to have a monoenergetic or near-monoenergetic character. Excitation and ionization cross sections are velocity dependent, rather than energy dependent quantities. A mix of electrons, protons, and heavier ions precipitating into the atmosphere will have a wide range of velocities and deposit energy over a broad range of altitudes, as suggested by the auroral spectra of Figure 11. It is very likely on this basis that the precipitation would appear in measurable EUV radiation.

An alternative suggestion (SBS) that low-energy electrons may dissociate H_2 (reaction (R2), Table 1) without measurably affecting the H_2 Rydberg bands is difficult to defend. The H_2 (E,F) cross section leading to the production of H_2 Lyman bands has a strong peak in the 17- to 18-eV range [Ajello et al., 1984], whereas the neutral dissociation (reaction (R2)) cross section peaks in the range 15- to 16-eV from an 8.8-eV threshold. The production efficiency of the H_2 (E,F) state therefore tends to follow that of neutral dissociation to low electron temperatures, as shown in Figure 12. If we require an order of magnitude increased production of dissociated hydrogen in the active sector, at an electron temperature of $T_e = 4 \times 10^4$ K (3.4 eV), the H_2 Lyman bands would show a very measurable 2- to 3-kR increase in intensity. Reducing the electron temperature below 4×10^4 K as a means of discriminating against the H_2 bands increases the fractional amount of electron energy entering the direct heating process as opposed to dissociation. Presumably at some point it will be difficult to find a means of keeping the upper atmospheric temperature cooled to the observed value (T = 1000 K) or to keep electron densities down to reality in this scenario.

Conclusions

1. Analysis of the Voyager EUV equatorial spectra of the sunlit atmosphere of Jupiter are consistent with an approximately constant relative abundance of atomic hydrogen as a function of magnetic longitude. This result does not support earlier explanations of the H Ly α variation with magnetic longitude on the basis of a proposed correlated variation in atomic hydrogen abundance.

2. An explanation for the H Ly α asymmetry is advanced on the basis that a variable ionospheric density may cause preferential collisional production of H(2p) atoms through the H(2s) → H(2p) transition, and variable production of H(2s) and H(2p) atoms through the recombination of H_2^+ and H_3^+. All of the necessary conditions and quantities for these processes appear to be present in Jupiter's exosphere.

3. The explanation for the H Ly α asymmetry advanced here requires very little energy to create the phenomenon in contrast to earlier explanations. However, the phenomenon in this analysis is a symptom of a process depositing a substantial amount of energy in the exosphere that cannot be explained by deposition of solar radiation. On the other hand the evidence suggests that energy deposition is controlled by solar photons as a catalyst both in the long-term 11-year solar cycle and in day-night relationships.

4. Energy deposition in the exosphere of Jupiter is at a level sufficient to control ionospheric densities and probably determines the upper atmospheric temperature, just as a similar process controls the upper atmospheric temperature on Saturn. Phenomenologically similar processes occur on Saturn and Titan, but our understanding is at such a rudimentary level that it is not at all clear they are similar in an epistemological sense. The origin of the exospheric activity appears to be one of the more important subjects for further study.

5. A large fraction (>50%) of the H Ly α emission from the sunlit hemisphere of Jupiter and Saturn is electron excited at least at the time of solar maximum in the 11-year cycle. Estimates of eddy diffusion coefficients have been

based on the assumption that emissions were entirely produced by solar resonance scattering, and calculations should be revised if the present results are accepted.

6. The H_2^+ and H_3^+ in the middle and outer magnetosphers of Jupiter and Saturn are probably supplied from the sunlit exospheric reactions described here, in accord with the conclusions drawn by the Voyager LECP experimenters.

Acknowledgements. The author has benefited from discussions with a number of colleagues, notably G. R. Smith, J. C. McConnell, G. R. Gladstone, A. J. Dessler, Y. L. Yung, R. A. Brown, B. Sandel, and J. M. Ajello. R. A. Brown made a special contribution by pointing out the important work of J. D. Purcell. Critical readings of the paper by D. F. Strobel and D. M. Hunten are much appreciated. W. T. Forrester and T. McBreen provided valuable support in Voyager data reduction. This work is supported by NASA, Division of Planetary Sciences, grant NAGW-106, to the University of Southern California.

The Editor thanks the two referees for their assistance in evaluating this paper.

References

Acuña, M. H., and N. F. Ness, Results from the GSFC fluxgate magnetometer on Pioneer 11, in Jupiter, edited by T. Gehrels, p. 830, University of Arizona Press, Tucson, 1976.

Ajello, J. M., D. E. Shemansky, T. L. Kwok, and Y. L. Yung, Studies of extreme-ultraviolet emission from Rydberg series of H_2 by electron impact, Phys. Rev. A, 29, 636, 1984.

Ashihara, O., Methane photochemistry in the outer planets, Rep. 602, The Inst. of Space and Astronaut. Sci., Tokyo, Feb. 1983.

Atreya, S. K., M. C. Festou, T. M. Donahue, R. B. Kerr, E. S. Barker, W. D. Cochran, J. L. Bertaux, and W. L. Upson, II, Copernicus measurement of the Jovian Lyman-alpha emission and its aeronomical significance, Astrophys. J., 262, 377, 1982.

Auerback, D., R. Cacak, R. Caudano, T. D. Gaily, C. J. Keyser, J. W. McGowan, J. B. A. Mitchell, and S. F. J. Wilk, Merged electron-ion beam experiments, I, Method and measurements of $(e-H_2^+)$ and $(e+H_3^+)$ dissociative-recombination cross sections, J. Phys. B, 10, 3797, 1977.

Bates, D. R., A. E. Kingston, and R. W. P. McWhirter, Recombination between electrons and atomic ions, I, Optically thin plasmas, Proc. Roy. Soc. London, 267, 297, 1962.

Bottcher, C., Dissociative ionization of the hydrogen molecule, J. Phys. B, 7, 2352, 1974.

Broadfoot, A. L., et al., Overview of the Voyager ultraviolet spectrometry results through Jupiter encounter, J. Geophys. Res., 86, 8259, 1981.

Brown, R. L., and W. G. Mathews, Theoretical continuous spectra of gaseous nebulae, Astrophys. J., 160, 939, 1970.

Burke, P. G., A. J. Taylor and S. Ormonde, Low-energy electron scattering by atomic hydrogen, III, Comparison of theory and experiment for the electron-induced excitation of hydrogen to the n = 2 level, Proc. Phys. Soc., 92, 345, 1967.

Carlson, R. W., H. S. Ogawa, E. Phillips, and D. L. Judge, An absolute measurement of the extreme ultraviolet solar flux, Appl. Opt., 23, 2327, 1984.

Carnahan, B. L. and E. C. Zipf, Dissociative excitation of H_2, HD, and D_2 by electron impact, Phys. Rev. A, 16, 991, 1977.

Clarke, J. T., H. A. Weaver, P. D. Feldman, H. W. Moos, W. F. Fastie, and C. B. Opal, Spatial imaging of hydrogen Lyman emission from Jupiter, Astrophys. J., 240, 696, 1980a.

Clarke, J. T., H. W. Moos, S. K. Atreya, A. L. Lane, Observations from earth orbit and variability of the polar aurora on Jupiter, Astrophys. J. Lett., 241, 179, 1980b.

Clarke, J. T., H. W. Moos, and P. D. Feldman, IUE monitoring of the spatial distribution of the H Lyα emission from Jupiter, Astrophys. J. Lett., 245, 127, 1981.

Clarke, J. T., H. W. Moos, and P. D. Feldman, The far-ultraviolet spectra and geometric albedos of Jupiter and Saturn, Astrophys. J., 255, 806, 1982.

Comes, F. J., and V. Wenning, Photoinduzierte Stossprozesse metastabiler Wasserstoffatome mit H_2 im Energiebereich von 0,05-0,47 eV, Z. Naturforsch. A, 24, 587, 1969a.

Comes, F. J. and V. Wenning, Die Energieabhangigkeit der Chemie-Ionisations-Reaktion $H(2s) + H_2 \rightarrow H_3^+ + e^-$, Z. Naturforsch. A, 24, 1227, 1969b.

Comes, F. J. and V. Wenning, Photodissociation of H_2 near threshold energies, Z. Naturforsch. A, 25, 237, 1970.

Crowe, A., and J. W. McConkey, Dissociative ionization by electron impact, I, Protons from H_2, J. Phys. B, 6, 2088, 1973.

Dalgarno, A. and A. C. Allison, Photodissociation of molecular hydrogen on Venus, J. Geophys. Res., 74, 4178, 1969.

Dance, D. F., M. F. A. Harrison, R. D. Rundel, and A. C. H. Smith, A measurement of the cross section for proton production in collisions between electrons and H_2^+ ions, Proc. Phys. Soc., 92, 577, 1967.

Dessler, A. J, and V. M. Vasyliunas, The magnetic anomaly model of the Jovian magnetosphere: Predictions for Voyager, Geophys. Res. Lett. 6, 37, 1979.

Dessler, A. J., B. R. Sandel, and S. K. Atreya, The Jovian hydrogen bulge: Evidence for co-rotating magnetospheric convection, Planet. Space Sci., 29, 215, 1981.

Donnelly, R. F., and J. H. Pope, The 1-3000 A solar flux for a moderate level of solar activity for use in modeling the ionosphere and upper atmosphere, Tech. Rep. ERL 276-SEL25, Natl. Oceanic and Atmos. Admin., Boulder, Colo., 1973.

Dunn, G. H., Franck-Condon factors for the ionization of H_2 and D_2, J. Chem. Phys., 44, 2592, 1966.

Dunn, G. H. and B. Van Zyl, Electron impact dissociation of H_2^+, Phys. Rev., 154, 40, 1967.

Freund, R. S., J. A. Schiavone, and D. F. Brader, Dissociative excitation of H_2: Spectral line shapes and electron impact cross sections of the Balmer lines, J. Chem. Phys., 64, 1122, 1976.

Gladstone, G. R., The radiative transfer of resonance lines with internal sources, J. Quant.

Spectrosc. Radiat. Transfer, in press, 1984.
Gladstone, G. R., and Shemansky, D. E., Radiative transfer of internal sources: Application to the Lyman α dayglow of Jupiter, Bull. Am. Astron. Sco., 15, 832, 1983.
Gladstone, G. R., and Y. L. Yung, An analysis of the reflection spectrum of Jupiter from 1500 Å to 1740 Å, Astrophys. J., 266, 415, 1983.
Glasstone, S., K. J. Laidler, and H. Eyring, The Theory of Rate Processes, The Kinetics of Chemical Reactions, Viscosity, Diffusion and Electrochemical Phenomena, edited by L. P. Hammett, pp. 220, McGraw-Hill, New York, 1941.
Guyon, P. M., J. Breton, and M. Glass-Maujean, Predissociation of the $^1\Pi_u^+$ states of H_2: Measurement of the various dissociation yields, Chem. Phys. Lett., 68, 314, 1979.
Hamilton, D. C., G. Gloeckler, S. M. Krimigis, C. O. Bostrom, T. P. Armstrong, W. I. Axford, C. Y. Fan, L. J. Lanzerotti, and D. M. Hunten, Detection of energetic hydrogen molecules in Jupiter's magnetosphere by Voyager 2: Evidence for an ionospheric plasma source, Geophys. Res. Lett., 7, 813, 1980.
Hamilton, D. C., G. Gloeckler, S. M. Krimigis, and L. J. Lanzerotti, Composition of nonthermal ions in the Jovian magnetosphere, J. Geophys. Res., 86, 8301, 1981.
Hamilton, D. C., D. C. Brown, G. Gloeckler, and W. I. Axford, Energetic atomic and molecular ions in Saturn's magnetosphere, J. Geophys. Res., 88, 8905, 1983.
Hazi, A. U., Comment on the dissociative ionization of H_2, J. Phys. B Lett., 8, 262, 1975.
Heddle, D. W. O., Photon scattering processes, J. Quant. Spectrosc. Radiat. Transfer, 2, 349, 1962.
Herbst, E., and W. Klemperer, The formation and depletion of molecules in dense interstellar clouds, Astrophys. J., 185, 505, 1973.
Hill, T. W., A. J. Dessler, and C. K. Goertz, Physics of the Jovian Magnetosphere, edited by A. J. Dessler, pp. 353-395, University Press, Cambridge, 1983.
Huntress, W. T., A review of Jovian ionospheric chemistry, in Adv. At. Mol. Phys., 10, 295, 1974.
Johnson, R., and M. A. Biondi, Measurements of positive ion conversion and removal reactions relating to the Jovian ionosphere, Icarus, 23, 139, 1974.
Julien, J., M. Glass-Maujean, and J. P. Descoubes, On the dissociation of the H_2 molecule following electron impact and leading to the obtention of atomic hydrogen in the n = 3 levels, J. Phys. B Lett. 6, 196, 1973.
Kieffer, L. J., and G. H. Dunn, Electron impact ionization cross-section data for atoms, atomic ions, and diatomic molecules, I, Experimental data, Rev. Mod. Phys., 38, 1, 1966.
Kingston, A. E., W. C. Fon, and P. G. Burke, The 1s - 2s and 1s - 2p excitation of atomic hydrogen by electron impact, J. Phys. B, 9, 605, 1976.
Kulander, K. C., and M. E. Guest, Excited electronic states of H_3 and their role in the dissociation recombination of H_3^+, J. Phys. B Lett., 12, 501, 1979.
Lee, L. C., R. W. Carlson and D. L. Judge, The absorption cross sections of H_2 and D_2 from 180 to 780 Å, J. Quant. Spectrosc. Radiat. Transfer, 16, 873, 1976.
Leventhal, M., R. T. Robiscoe, and K. R. Lea, Velocity distribution of metastable H atoms produced by dissociative excitation of H_2, Phys. Rev., 158, 49, 1967.
Mathur, D., S. U. Khan, and J. B. Hasted, Dissociative recombination in low energy e-H_2^+ and e-H_3^+ collisions, J. Phys. B, 11, 3615, 1978.
McConnell, J. C., B. R. Sandel, and A. L. Broadfoot, Airglow from Jupiter's nightside and crescent: Ultraviolet spectrometer observations from Voyager 2, Icarus, 43, 128, 1980.
McConnell, J. C., B. R. Sandel, and A. L. Broadfoot, Voyager ultraviolet spectrometer observations of He 584 Å dayglow at Jupiter, Planet. Space Sci., 29, 283, 1981.
McConnell, J. C., J. B. Holberg, G. R. Smith, B. R. Sandel, D. E. Shemansky, and A. L. Broadfoot, A new look at the ionosphere of Jupiter in the light of the EUV occultation results, Planet. Space Sci., 30, 151, 1982.
Misakian, M. and J. C. Zorn, Dissociative excitation of molecular hydrogen by electron impact, Phys. Rev. A, 6, 2180, 1972.
Mitchell, J. B. A., J. L. Forand, C. T. Ng, D. P. Levac, R. E. Mitchell, P. M. Mul, W. Claeys, A. Sen, and J. W. McGowan, Measurement of the branching ratio for the dissociative recombination of H_3^+ + e, Phys. Rev. Lett., 51, 885, 1983.
Mumma, M. J. and E. C. Zipf, Dissociative excitation of vacuum ultraviolet emission features by electron impact on molecular gases, I, H_2 and O_2, J. Chem. Phys., 55, 1661, 1971.
Newman, J. H., J. D. Cogan, D. L. Ziegler, N. E. Nitz, R. D. Rundel, K. A. Smith, and R. F. Stebbings, Charge transfer in H^+-H and H^+-D collisions within the energy range 0.1-150 eV, Phys. Rev. A, 25, 2976, 1982.
Osterbrock, D. E., Astrophysics of Gaseous Nebulae, W. H. Freeman, San Francisco, Calif., 1974.
Peart, B. and K. T. Dolder, Collisions between electrons and H_2^+ ions, V, Measurement of cross sections for dissociative recombination, J. Phys. B, 7, 236, 1974a.
Peart, B. and K. T. Dolder, Measurements of the dissociative recombination of H_3^+ ions, J. Phys. B, 7, 1948, 1974b.
Peek, J. M., Theory of dissociation of H_2^+ by fast electrons, Phys. Rev., 154, 52, 1967.
Peek, J. M., and T. A. Green, Improvement in the first Born theory of electron scattering by molecular systems, II, Example of the $1s\sigma_g$ - $2p\sigma_u$ transition in H_2^+, Phys. Rev., 183, 202, 1969.
Purcell, E. M., The lifetime of the $2\ ^2S_{1/2}$ state of hydrogen in an ionized atmosphere, Astrophys. J., 116, 457, 1952.
Sandel, B. R., A. L. Broadfoot, and D. F. Strobel, Discovery of a longitudinal asymmetry in the H Lyman-alpha brightness of Jupiter, Geophys. Res. Lett., 7, 5, 1980.
Shemansky, D. E. and J. M. Ajello, The Saturn spectrum in the EUV - electron excited hydrogen, J. Geophys. Res., 88, 459, 1983.
Shemansky, D. E. and G. R. Smith, The Voyager 1 EUV spectrum of the Io plasma torus, J. Geophys. Res., 86, 9179, 1981.
Shemansky, D. E. and G. R. Smith, Whence comes the 'Titan' hydrogen torus (abstract), EOS Trans. AGU, 63, 1019, 1982.

Skinner, T. E., S. T. Durrance, P. D. Feldman, and H. W. Moos, Temporal variation of the Jovian HI Lyman-alpha emission (1979-1982), Astrophys. J. Lett., 265, 23, 1983.

Smith, G. R., D. E. Shemansky, J. B. Holberg, A. L. Broadfoot, and B. R. Sandel, Saturn's upper atmosphere from the Voyager 2 EUV solar and stellar occultations, J. Geophys. Res., 88, 8667, 1983.

Stephens, T. L., and A. Dalgarno, Spontaneous radiative dissociation in molecular hydrogen, J. Quant. Spectrosc. Radiat. Transfer, 12, 569, 1972.

Stephens, T. L., and A. Dalgarno, Kinetic energy in the spontaneous radiative dissociation of molecular hydrogen, Astrophys. J., 186, 165, 1973.

Strobel, D. F., and D. E. Shemansky, EUV emission from Titan's upper atmosphere: Voyager 1 encounter, J. Geophys. Res., 87, 1361, 1982.

Vasyliunas, V. M., and A. J. Dessler, The magnetic-anomaly model of the Jovian magnetosphere: A post-Voyager assessment, J. Geophys. Res., 86, 8435, 1981.

Vroom, D. A., and F. J. de Heer, Production of excited atoms by impact of fast electrons on molecular hydrogen and deuterium, J. Chem. Phys., 50, 580, 1969.

Waite, J. H., T. E. Cravens, J. Kozyra, A. F. Nagy, S. K. Atreya, and R. H. Chen, Electron precipitation and related aeronomy of the Jovian themosphere and ionosphere, J. Geophys. Res., 88, 6143, 1983.

Yung, Y. L., G. R. Gladstone, K. M. Chang, J. M. Ajello, and S. K. Srivastava, H_2 fluorescence spectrum from 1200 to 1700 A by electron impact: Laboratory study and application to Jovian aurora, Astrophys. J. Lett., 254, 65, 1982.

D. E. Shemansky, Lunar and Planetary Laboratory, University of Arizona, Tucson, AZ 85713, (602) 621-4301.

(Received June 13, 1984;
revised October 1, 1984;
accepted October 24, 1984.)